CORRELATING THE EFFECTS OF AP PARTICLE SIZE AND CONCENTRATION ON AP/HTPB COMPOSITE PROPELLANT BURNING RATES

A Thesis

by

GORDON R MORROW

Submitted to the Office of Graduate and Professional Studies of
Texas A&M University
in partial fulfillment of the requirements for the degree of

MASTER OF SCIENCE

Chair of Committee,	Eric L. Petersen
Committee Members,	Adonios N. Karpetis
	Timothy Jacobs
Head of Department,	Andreas A. Polycarpou

May 2017

Major Subject: Mechanical Engineering

ABSTRACT

The burning rates of IPDI-cured AP/HTPB propellants with a standard curing ratio were analyzed. It is well known that the particle size of AP as well as their concentration greatly affects the burning rate, yet there exists a lack of archival databases for a wide range of particle sizes, concentrations and pressures. Testing conditions for this study included an average AP size range of 20 μm – 400 μm with four intermediate steps, a pressure range of 500 - 2,250 psi with multiple intermediate steps, and lastly a concentration range of 70% to 85% AP by mass with three intermediate steps. As expected, decreasing the AP size increased the burning rate for sizes above about 45 μm and increasing the concentration of AP led to an increase in burning rate. The results for the smaller sizes (20 and 45 μm) converged to similar burning rates, indicating that the mixture is nearing a premixed burning limit.

All propellants were manufactured and tested in house at Texas A&M using the same experimental techniques and testing procedures used in the past by previous authors. Power law burning rate expressions were obtained for each mixture. Most importantly, an empirical correlation describing the burning rates over the entire range of propellants tested was created by analyzing the trends seen in the pressure coefficient and exponent of each propellant formulation. The correlation was built off of multiple data sets. These data sets include data taken by the author at TAMU, data taken by Kohga, King, and Foster. The correlation was applied and compared to multiple data sets

and produced good agreement with an R-squared value of 0.968. The advantage of this correlation over other theoretical models is primarily its simplicity and accuracy. Its form mirrors the well-known power law which makes it easily adoptable as a potential replacement.

The correlation also has a large potential for future modification and adjustment. In the future, these same formulations should be tested between the 2,250 to 5,000 psi ranges where the role of AP becomes crucially important. Catalytic effects of additives should also be included as additional terms in the pressure coefficient and exponent as well as the effect that initial propellant temperature has on burning rate.

ACKNOWLEDGMENTS

I would first like to thank my committee chair and advisor Dr. Eric Petersen for making this even possible. I would also like to thank all my committee members, Dr. Tim Jacobs and Dr. Adonios Karpetis, for giving their time to this thesis.

Over the past two years I have also received an overwhelming amount of instruction and friendship from those researchers who also work at Dr. Eric Petersen's laboratories. Much of what I done would not have been possible without individuals such as Andrew Demko, Jacob Stahl, Catherine Dillier, James Thomas, and Thomas Sammet. I sincerely thank you all.

Thanks also go to my friends and colleagues and the department faculty and staff for making my time at Texas A&M University a great experience.

The support my family has offered throughout my entire academic career cannot be measured with words. Their encouragement and friendship has made this journey an immeasurable joy. And without my father in particular none of this would ever have even happened. I would not have the desire to understand God's universe nor the will to strive for excellence if it were not for him, thank you.

CONTRIBUTORS AND FUNDING SOURCES

This work was supervised by a thesis committee consisting of my advisor Professor Eric Petersen and Professor Timothy Jacobs of the Department of Mechanical Engineering and Professor Adonios Karpetis of the Department of Aerospace Engineering at TAMU.

The AP particle size information in Chapter 3 was provided by colleague Andrew Demko. Burning rate measurements in Chapter 4 for the 80%, 400-µm AP formulation were conducted in part by Andrew Tykol and Andrew Demko of the Department of Mechanical Engineering. Burning rate measurements in Chapter 4 for the 80%, 200-µm AP and 20-µm AP were provided from numerous researchers at Dr. Eric Petersen's laboratory.

APCP Exponent break information in future works was collected by James Thomas of the Department of Mechanical Engineering at TAMU. Recreated graphs from Foster, King, and Khuga were also developed by James Thomas. James also helped in the development of the non-linear regression correlation.

All other work conducted for the thesis was completed by the student in collaboration with advisor Dr. Eric Petersen of the Department of Mechanical Engineering at Texas A&M University.

There are no outside funding contributions to acknowledge related to the research and compilation of this document.

NOMENCLATURE

a	Burning rate constant (also called the pressure coefficient)
AP	Ammonium perchlorate
APCP	Ammonium perchlorate composite propellant
BDP	Beckstead-Derr-Price
BR	Burning rate
DAQ	Data acquisition
HTPB	Hydroxyl-terminated polybutadiene
IPDI	Isophorone Diisocyanate
n	Burning rate pressure exponent
PEM	Petite ensemble model
PSU	Power supply
SRB	Solid rocket booster
TAMU	Texas A&M University

TABLE OF CONTENTS

LIST OF FIGURES

Page

LIST OF TABLES

Page

CHAPTER I

INTRODUCTION

APCP's for the last half century have been the propellants of choice when the application of solids is needed; finding use in missiles, airbags, aircraft ejection seats, and more notably the space shuttle's SRB's and rocketry in general [1]. They boast an enormous amount of thrust compared to other types of rockets of similar size and a relatively high specific impulse (I_{sp}) of 285 seconds under vacuum in the case of the Titan IVB SRMU [2].

An important aspect of APCP's is their simplicity. They are composed of a single oxidizing agent, AP, a rubbery binder that serves both as structural support for the propellant grain and fuel for combustion, and finally additives which are used to tailor certain characteristics to specific application needs. In the case of this study, HTPB was chosen for the binder over others because of its desirable mechanical properties and common usage [3]. Typical additives include catalysts, used to increase burning rate and hence thrust, and strengthening additives like Tepanol. A representation of a typical propellant cross section is provided in Fig. 1, although the effects of additives were not studied for the present research.

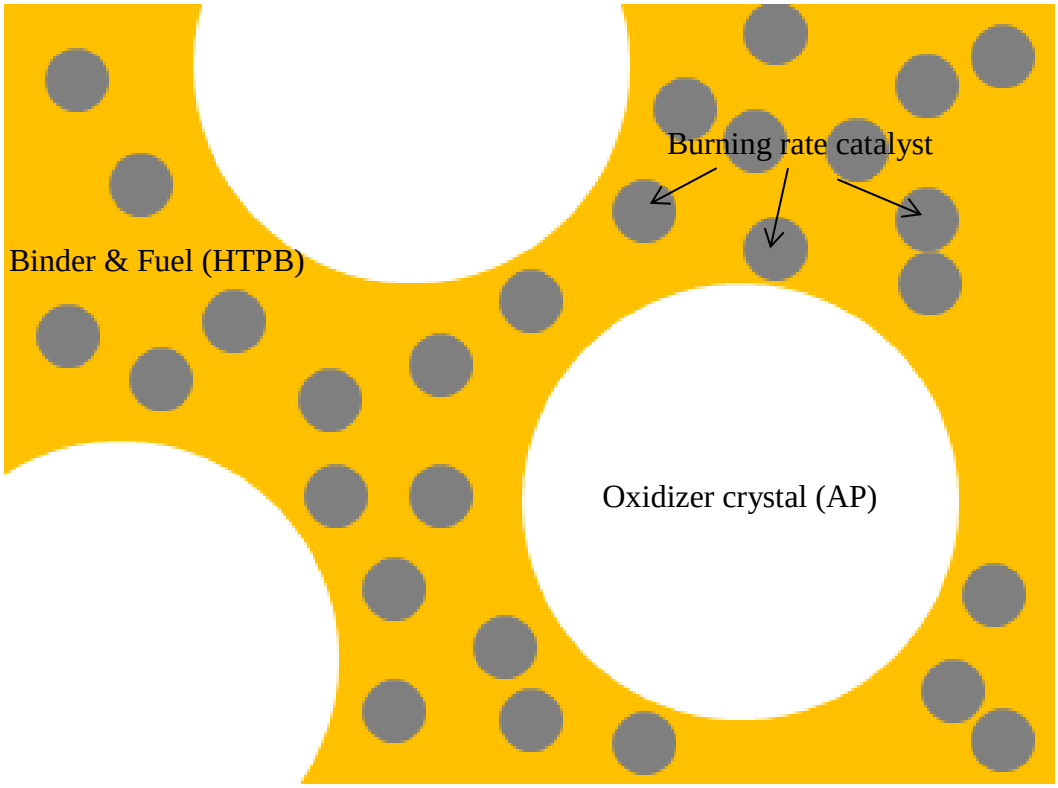

Figure 1: Propellant cross section with a single average AP size.

A very important factor to control when dealing with solid propellants is the burning rate. Because the combustion of composite propellants is rather complicated, it is common practice to approximate the burning rate using the well-known power law as shown in Eqn. 1 [4]. The constants *a* and *n* are empirically determined and are unique for every propellant formulation.

$$BR = aP^n \tag{1}$$

For a fixed nozzle, the burning rate ties into what the chamber pressure will be. The faster a propellant burns and gasifies the more mass flow of gas is realized through the chamber containing the propellant, thereby increasing chamber pressure. This is an important parameter to control, primarily for safety. Engineers must design a case to withstand the pressure of the gas pushing against the side wall. It is also crucially important for nozzle design, combustion instability, as well as many other aspects for rocketry. Naturally it then becomes the question to ask what sort of things, other than pressure, composition, and temperature, can affect burning rate. For some time, researchers have known that the size or diameter of the AP particles within the binder matrix can have an equal or even greater impact on burning rate than their concentration alone. For example, Fig. 2 shows a historical graph of data taken at the author's laboratory at Texas A&M University (TAMU) which demonstrates the impact of AP particle diameter on burning rate. As seen, changing the average AP particle size from 200 down to 20 microns increases the burning rate by a factor of about 3 to 4. Surprisingly however, there are few sources in the open literature that contain well-documented data sets on the effect of AP particle size and concentration on the burning rate of AP/HTPB composite propellants over a wide pressure range.

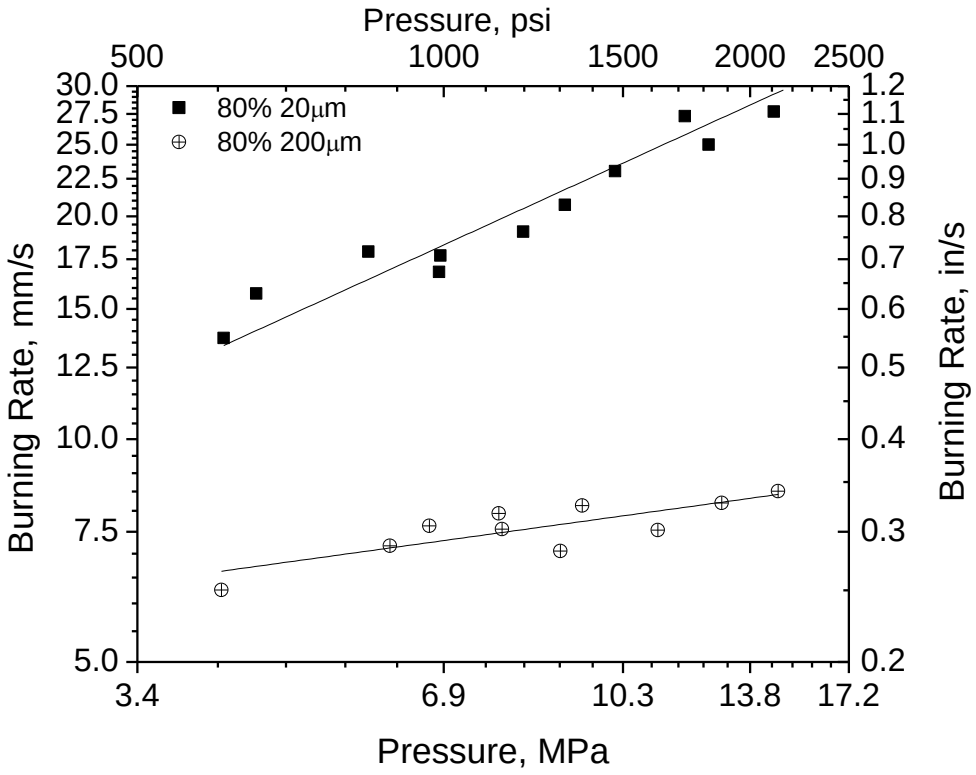

Figure 2: Typical effect of AP particle size on the burning rate of composite propellants.

The objective for the present work was to provide a source of modern burning rate data and also to correlate the resulting trends as a function not only of pressure, but of particle size and concentration as well and to do it in an easy-to-use format that mirrors that of the power law. Such data should be useful for estimation purposes as well as for accessible archival data for numerical models of the solid propellant combustion process. The end result is a comprehensive function that researchers can use to better model chamber pressure within a rocket, or some other combustion-related process without having to either gather specific baseline data themselves or go searching for available references.

$$a = a(\mathrm{D}, \mathrm{C}) \tag{2}$$

$$n = n(\mathrm{D}, \mathrm{C}) \tag{3}$$

Equation 2 demonstrates how the pressure coefficient *a* from the power law (E.q 1) will be correlated as a function of AP mean diameter and overall concentration. The same holds true for the pressure exponent *n* in equation 3. Because the correlation will use fitted constants it will be imperative that the proper units are used. The term P is pressure in psi, D is AP particle diameter in microns, and C is the concentration of AP in decimal form like so (0.XX). Once the pressure coefficient and exponent are calculated, they can be placed into the power law Eq. (1) and the burning rate obtained therefrom.

The advantage of such a correlation over other theoretical models is simplicity. With this correlation, engineers will not be able to make insights into the true nature of APCP combustion, like with others, but what they are able to do is determine burning rate quickly and easily which makes it very useful on a practical rocket design level. It is the same reason the power law is so widely used. This correlation aims to extend the functionality of the popular power law without appreciably increasing its complexity.

Chapter two contains an in depth literature review which talks about previous modeling efforts in the rocket propellant community. The next chapter discusses the experimental approach taken for this study both the burning rate measurements and the techniques used to develop the correlation. In chapter four numerous data sets are

presented against the correlations prediction of the data set and comparisons are drawn. Finally in chapter five future work efforts are discussed followed by the conclusion.

CHAPTER II

BACKGROUND

As mentioned above, the burning rate dependence on AP particle size is not a new discovery. As far back as 1961, [5] for his thesis Bastress investigated the effects of AP size and concentration on burning rate across a wide range of pressure. It represents one of the most complete and detailed burning rate studies regarding APCP's, which has made it a highly referenced database still to this day. The study covers a range of 9-260 μm particle size and 65-80% concentration of AP tested across a pressure range of 30-1600 psi. Although the binder used in the study was polysulfide or polyester instead of HTPB, the general trends still hold true for AP-HTPB propellants. The general trends show an increase in burning rate as AP particle size is reduced and or its concentration is increased. Figure 3 and Figure 4 were taken from Bastress to give an example of these effects.

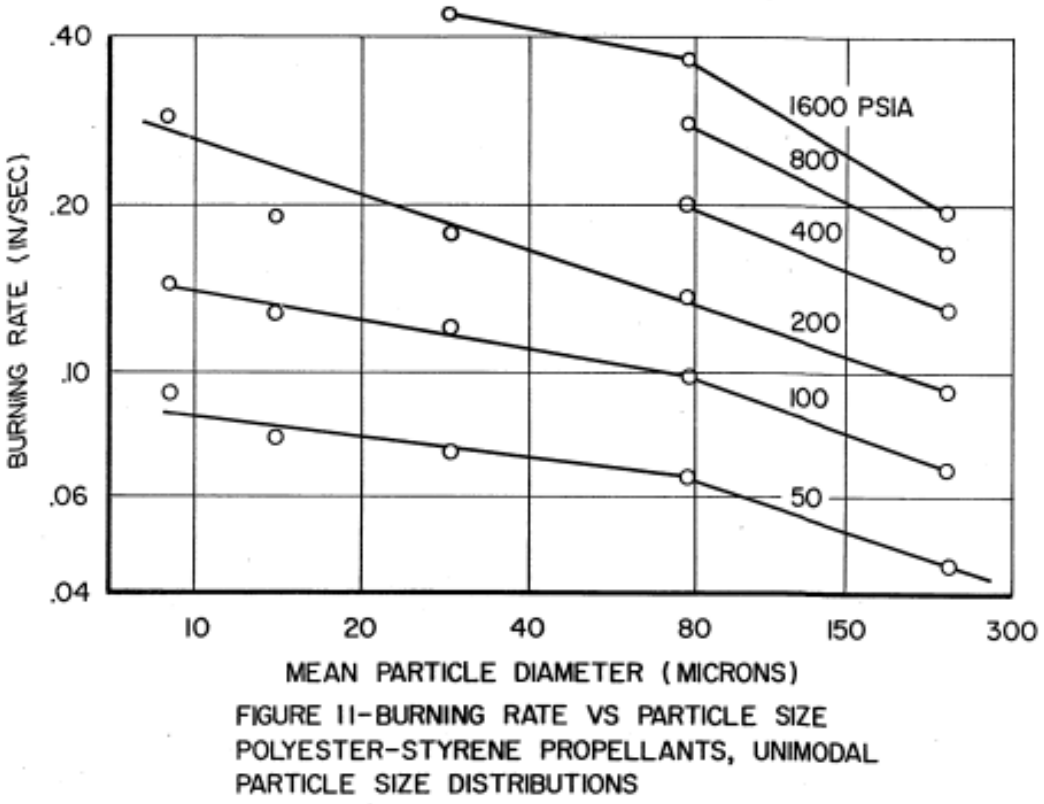

Figure 3: Deflagration rate for AP-Polyester propellant, taken directly from Bastress 1961, demonstrating the effect of AP particle size on the burning rate **[5]**.

In this first graph (Fig. 3), burning rate is plotted against mean particle diameter of the AP. Multiple curves are made which correspond to different test pressures which range from 50 to 1600 psi. The graph demonstrates two effects talked about previously. The first of which is the inverse relationship between burning rate and particle diameter, and the second is the proportional relationship between burning rate and test pressure.

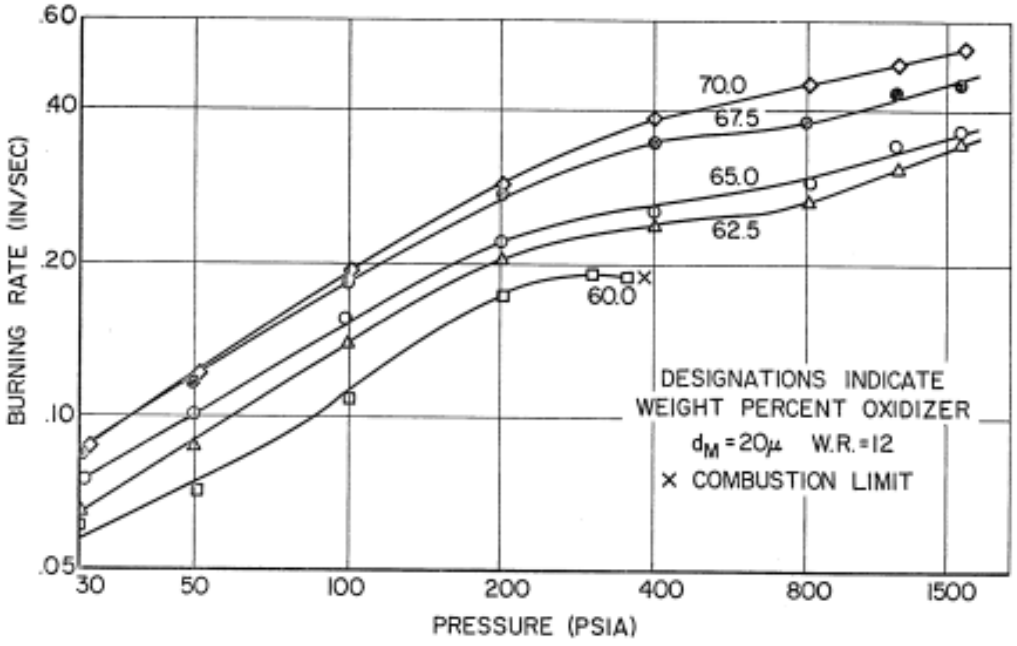

FIGURE 14 – BURNING RATE VS PRESSURE, POLYSULFIDE PROPELLANTS WITH VARYING OXIDIZER CONCENTRATION, FINE PARTICLES

Figure 4: Deflagration rate for AP-Polysulfide propellant taken directly from Bastress 1961, demonstrating the effect of AP concentration on the burning rate **[5]**.

In Figure 4, burning rate is plotted on the y axis against test pressure this time instead of AP particle size. Now, multiple cruves are made which correspond to different concentrations of AP by mass. The concentration ranges from 60% to 70%. Again, the same proportional relationship between burning rate and pressure is seen. But now a relationship between burning rate and concentration of AP is evident. All three of these variables, pressure, particle diameter, and concentration, produce effects that are now considered well known, but it is important to establish a historical baseline for when these trends were originally quantified.

From the observation by Bastress, there stemmed a large effort to understand and model these steady state APCP combustion trends. A pioneer in this modeling effort was Hermance [6] who was one of the first to consider these trends. As a first attempt, he simplified the process greatly which would later be built upon by Beckstead. Hermance first considered the heterogeneous reaction of the fuel and oxidizer decomposition products. Then the gas-phase flame position was calculated by taking into account diffusional mixing, these processes were then combined into a simple, one-dimensional energy balance which allowed for the calculation of the burning rate. The model proposed by Hermance showed moderate agreement against experimental trends, with error falling around the 10% mark.

Beckstead, Derr, and Price would add to this work by introducing the well-know DBP three-flame model [7]. This model would later be modified numerous times by both the Beckstead group and others [8] [9]. At its core, it was a leap in both understanding and modeling for APCP combustion mechanics.

The main innovation with the BDP model was that, instead of considering one flame zone surrounding a single AP crystal, it considered three. The first, like in the Hermance model, was the Primary flame between the decomposition products of the fuel (binder) and oxidizer. The Second was the premixed oxidizer flame because AP is truly a monopropellant [10], and the last was the final diffusion flame between the products of the first two flames.

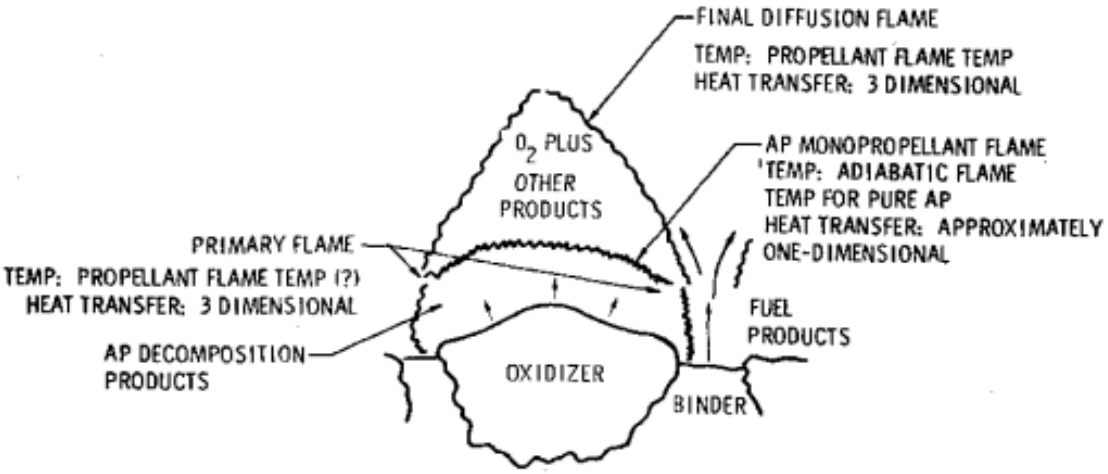

Figure 5: Illustration of the 3-flame model from BDP, taken directly from the original reference **[7]**.

Figure 5 illustrates the flame zones considered by the BDP model. Gas-phase reactions were modeled with kinetics, and surface decomposition was described with an Arrhenius expression. The model took into account AP particle size, concentration, initial temperature, and ambient pressure. In the initial study, they compared the model against experimental data that had an AP size range of 5-200 μm and concentrations between 60 and 70% by mass. A limitation to this first model was that it applied only to additive-free formulations with only one-size of spherical AP. However, this size limitation is rarely the case in modern propellant formulations, so improvements needed to be made.

Later Cohen [11] and his group would extend the functionality of this model to include both aluminized formulations and those with bi-modal distributions of AP. Around the same time as Beckstead et al.'s initial publication, a work done by [12]

investigated the effects of the AP size distribution. A distribution function was created that partitioned the particles into groups, and then the effects of each group of "pseudopropellant" were summed to get the overall behavior.

A competitor to the BDP model was developed by King [13] at the Atlantic Research Corporation. It borrowed many concepts from the BDP model but with major modifications. An important addition in King's model was the introduction of erosive burning which occurs when a high-speed gaseous cross flow is present near the surface of the burning propellant. Such a feature is thought to more accurately describe what propellant in a real rocket casing would experience.

These literature citations are just a few of the more-notable publications relating to composite propellant burning rate modeling during the 1970's. A comprehensive review done by Cohen [14] in 1980 provides great detail on the large amount of work done on this topic and thus is a great resource for further edification.

The common outcome from all these studies, again, was that decreasing the particle size leads to an increase in burning rate; and there existed an ideal range of AP concentration that returned the best I_{sp} and burning rate. Initial temperature, AP size distributions, and mode also have an effect on the propellant burning rate.

Since then, there have been numerous studies that continue to touch on this topic, such as Miller [15] and Norman [16]. A recent effort was conducted by Frazier [17] who also based his model on that of the BDP model with modifications. Frazier's model is successful in predicting baseline burning rates but again only to within 10% and higher when additives are included. In Frazier's study, particular interest was given to the

effects of nano-scale additives on the condensed-phase kinetics of the propellant. It was also the first model that tried predicting anomalous burning rate trends, such as plateaus and mesas, and in this regard the study is unique. But again being a theoretical model based on thermodynamics it can be cumbersome to use.

The models discussed thus far are primarily concerned with unimodal AP distributions. However, most modern formulations are rarely made in this way. Bi-modal or even tri-modal distributions of AP are typically used. A notable model in this area is the PEM model developed by Renie, Condon, and Osborn at Purdue University [10]. In this model, the effects of a bimodal distribution of AP was considered as well as the width of the individual peaks. Renie et al. also included effects of temperature although the real advancement here was how the size distribution of the AP was taken into account.

Not only are multi-mode distributions of AP harder to characterize, they have also been shown to sometimes produce “anomalous burning” which can be characterized as plateaus, mesas, and sometimes intermittent extinctions. These propellants do not follow a linear burning rate trend when plotted on a log-log scale [18], [19].

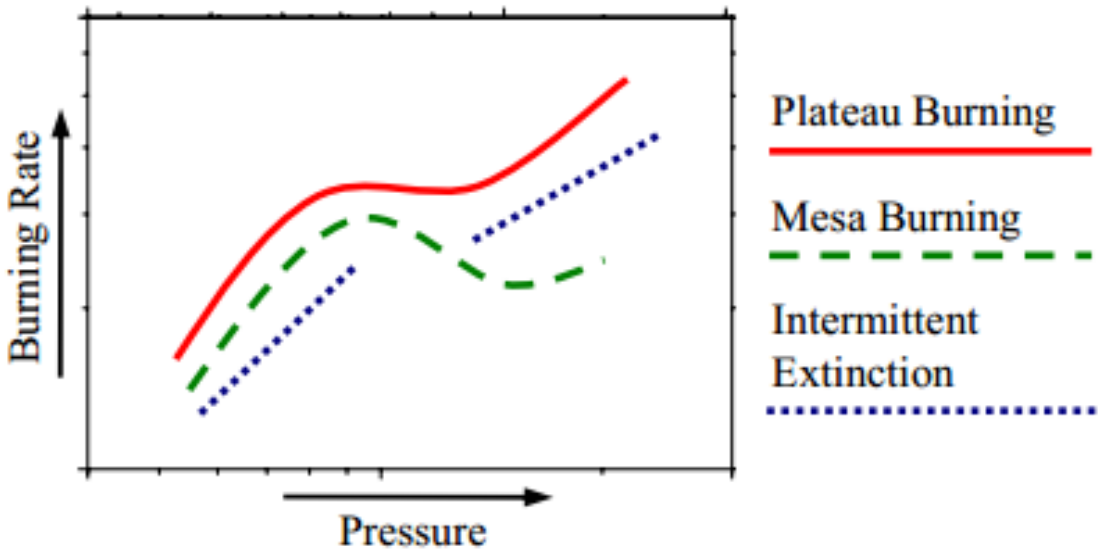

Figure 6: Typical behavior of anomalous propellants, taken directly from Stephens [19].

Figure 6 shows the typical behavior of plateau, mesa, and extinction propellants, and they do not follow liner trends. Figure 6 was adopted from Stephens [20]. The presence of this anomalous behavior further complicates the issue of understanding the underlying burning rate mechanism(s). [21] Boggs and his group were the first to observe the presence of a "Melt Layer" through the use of SEM which was believed to be the source of these plateau effects. Stephens targeted this topic and found that additives can be used to tailor this melt layer and hence the characteristics of the plateau, in his case. This finding again reinforces the fact that the burning of a composite propellant is incredibly complicated and still to this day not fully understood.

Despite the enormous efforts done to understand and model the burning rate mechanism of APCP's from a theoretical standpoint, little has been done in the open

literature to correlate burning rate trends from a purely empirical standpoint. The main downside to the models talked about thus far is that they are cumbersome to use from a practical standpoint. An engineer designing a rocket nozzle is faced with only a few options. One can try to exhaustively reproduce these theoretical models and still only get within 10% at best of the true burning rate. The engineer can attempt to dig through the open literature for historical burning rate data that applies to the exact, desired formulation, which is not always available. As a last resort, the engineer could build a small scale test stand or outsource the work to someone who already has one and test the formulation directly. All of these options are far from optimal.

The goal of this thesis work was to provide the rocket community with a database as it pertains to baseline AP/HTPB formulations across a wide range of pressure, particle size, and concentration. A second goal was to predict the burning rate trends with an empirically based correlation that that is simple to use. This practical tool will provide an option for engineers when attempting to predict the burning rate of a given APCP formulation.

Multiple sources of AP/HTPB composite propellant burning rate data were included in the development of the correlation to be seen later in this thesis. While it is important to correlate data collected at TAMU, it also adds weight to the validity of the model if it can predict burning rate data collected by others. Data collected by Kohga [22], King [23] and Foster [24] were thus chosen to be included in the current correlation development as their formulations resemble baseline APCPS and are similar to those

made at TAMU. Data from these authors was acquired from their graphs using photo editing software and as such they can only be considered an approximate representation.

CHAPTER III

EXPERIMENT

Key to the experiment was controlling the size of the AP particles. Because burning rate depends so heavily on the AP size, it was important to precisely control the average size; additionally, as seen from Miller, controlling its distribution was also important. Although AP can be commercially bought at various sizes, it is difficult to find vendors and even more difficult to guarantee precise distributions. Instead, AP was bought in bulk and sieved at TAMU using a mechanical sieve.

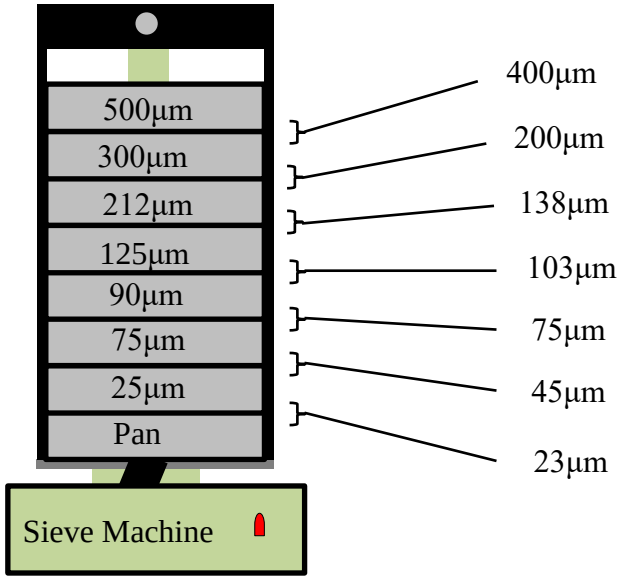

Figure 7: Mechanical sieve and sieve pan apparatus.

Figure 7 illustrates how the sieving process works. An array of sieves with known pore sizes is placed in the mechanical shaker. The raw AP is loaded in at the top, and the sieves are shaken for a period of 5 days, which is ample time for the AP to fall through the set of sieves. The particles only fall through sieves which have pore sizes larger than that of the AP particle. After the process is completed, the AP is collected from each sieve and the pan at the bottom. The sieve generally separates the raw AP into seven groups with a mean size that lies between the sieve in which it was collected and the one above. The AP is kept separate and then sent off to be sized before going into a propellant.

Figure 8 represents particle sizing data for the AP used in this study, which was collected at TAMU. The graph shows that the mechanical sieve was successful in producing highly uniform distributions of AP which is needed to accurately characterize baseline burning rates. On the x axis, particle size in microns is plotted on a log scale, and on the y axis is % volume on a linear scale. All particle sizing was done at Texas A&M University using an optical technique called Fraunhofer imaging.

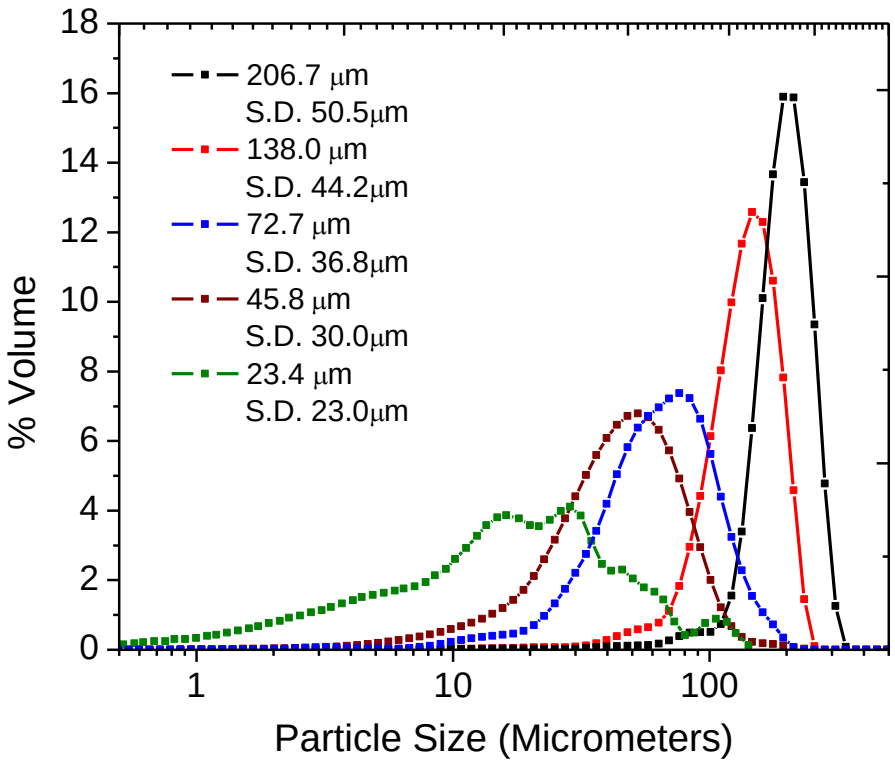

Figure 8: Measured AP size distribution graph, with average sizes and standard deviations (S.D.) identified.

Once the AP was properly sized and cataloged, the next step was the fabrication of the propellant itself. All propellants were made in house at Texas A&M University using standard procedures that were developed over years of research [25]. All liquid ingredients were first weighed and mixed together thoroughly. These ingredients consisted primarily of the HTPB binder, plasticizer, and a bonding agent as needed. The formulation was then put under a vacuum for at least thirty minutes to remove any air bubbles introduced during mixing. The dry ingredients, such as the AP oxidizer and

other powder additives, were then introduced and mixed thoroughly. Again the mixture was then put under vacuum to remove air bubbles. A cross linking agent, also called the curative, was the final ingredient in the mixture. IPDI was the curative for all formulations in this study, and only a small amount (0.3-0.4 g) was needed to set the NCO/OH ratio to one. Chemically the curative connects the local OH groups found on the ends of the HTPB chain; this is what turns the semi-solid material into a harder solid material. The final process was to cast the propellant in 3/16-inch inner diameter Teflon tubing. The tubing was manually pressed into the mixture and forced up into the tubing. This compression method gives the propellant a uniform shape that is ideal for linear burn rate calculations. Samples were cut to approximately one inch (25.4 mm) in length and set in an oven to accelerate the curing process. In the curing process, the oven holds the propellant at a temperature of 63ºC for one week. Figure 9 shows what a typical sample looked like after it had finished curing.

Figure 9: Picture of typical baseline AP/HTPB composite propellant manufactured at Texas A&M University.

Propellant formulations that have low concentrations, below 75%, of AP presented a particular challenge. Because AP has a higher density than HTPB it tends to sink towards the bottom of the Teflon tube while it sits in the oven. When the formulation with low AP concentration finishes curing, the AP particles are then locked in place all towards the one side of the propellant. This leads to poor combustion performance as the fuel-oxidizer local equivalence ratio is inconsistent throughout the propellant grain.

To reduce this effect, propellant formulations with low concentrations of AP were placed on a custom-built mechanical roller during the curing process. By doing

this, the AP particles were never allowed to settle towards one side of the Teflon tube. Once the binder finished curing, the particles were locked in place, and the roller was no longer needed. Figure 10 depicts the roller used in this study as well as a graphical representation of a propellant cross section in which the AP has settled.

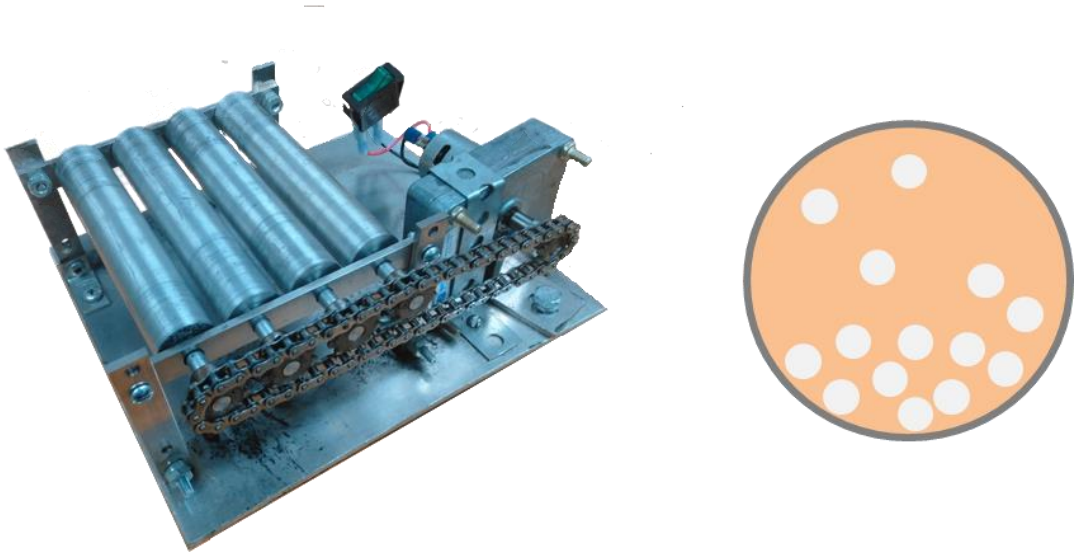

Figure 10: Mechanical roller used to reduce settling effects; Pictorial representation of settling effects in AP/HTPB binder fuel cross-section.

Once the propellant was through the manufacturing stage, it was then ready for testing. The propellant was burned in a high-pressure, constant-volume Crawford bomb (also called a strand burner). The strand burner was pressurized with an inert gas, such as Argon or Nitrogen. This inert gas eliminated any interference that oxygen in the air would have on the combustion process of the propellant strand. Typical testing pressures ranged from 500 psi to about 2300 psi, although the strand burner used at TAMU can

perform tests up to 5000 psi. It also has four windows which can be equipped with diagnostic equipment, such as a photodiode for light traces, a spectrometer, or a high-speed camera.

The samples were mounted on a modified bolt which was then screwed into the bottom of the strand bomb, sealing it inside. Small electrodes were mounted on either side of the propellant, and a small nichrome wire was attached to these electrodes and then pressed into the propellant surface. A power supply passes high current through the small wire, causing it to heat up. This heat is what ignites the propellant strand and starts the test. Figure 11 is a picture of the strand bomb and modified bolt used to collect the data. The strand bomb used for this study was designed and built by Dr. Eric Petersen's research group and resides at TAMU [26].

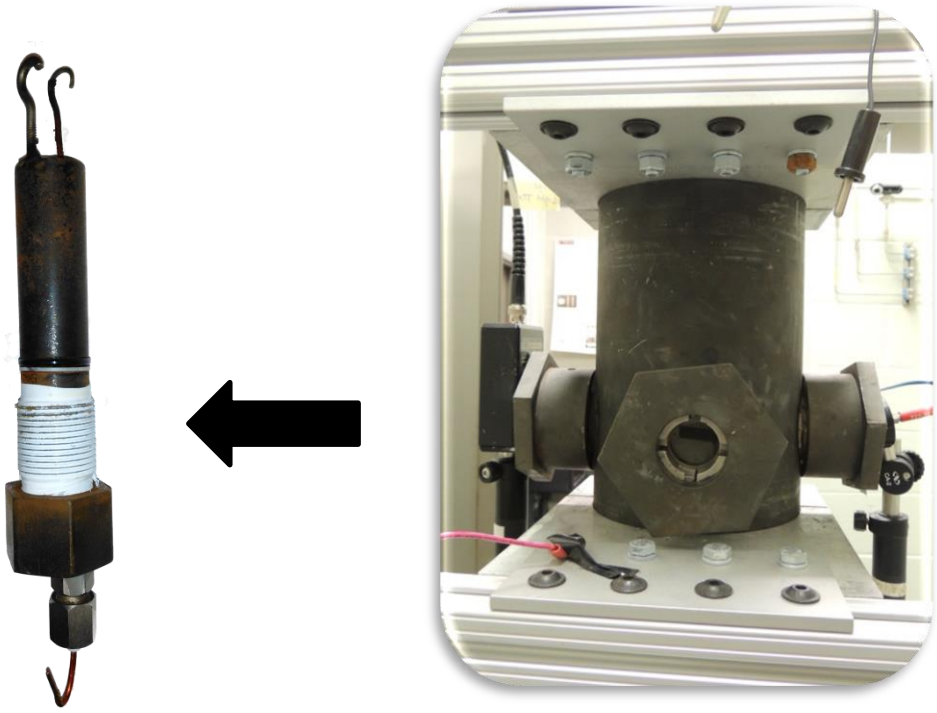

Figure 11: Modified bolt and high-pressure strand burner used to obtain propellant burning rates.

To begin a test, the propellant sample was first measured using digital calipers before it was burned; this will be important later when calculating average burning rate. Mass was also measured with a simple scale, and the sample was then rolled in un-cured HTPB. This thin layer of HTPB inhibits the side of the propellant from burning before the center of the propellant. This inhibiter is needed to make the assumption of a linear burn. From here, the sample was mounted on the modified bolt and screwed into the strand bomb. Once the bolt was secured in the strand bomb, all personnel leave the room and where the strand bomb is enclosed within a concrete-reinforced room designed to

contain the vessel in the event of a pressure-induced failure. The strand burner was then pressurized to the desired test pressure remotely through the use of electronically controlled solenoids. Once the strand bomb was at the desired test pressure, the circuit connecting the power supply to the small nichrome wire was completed which started the burning process. Figure 12 shows the schematic for this testing system. More information on the testing apparatus can be found in previous studies **[27]**.

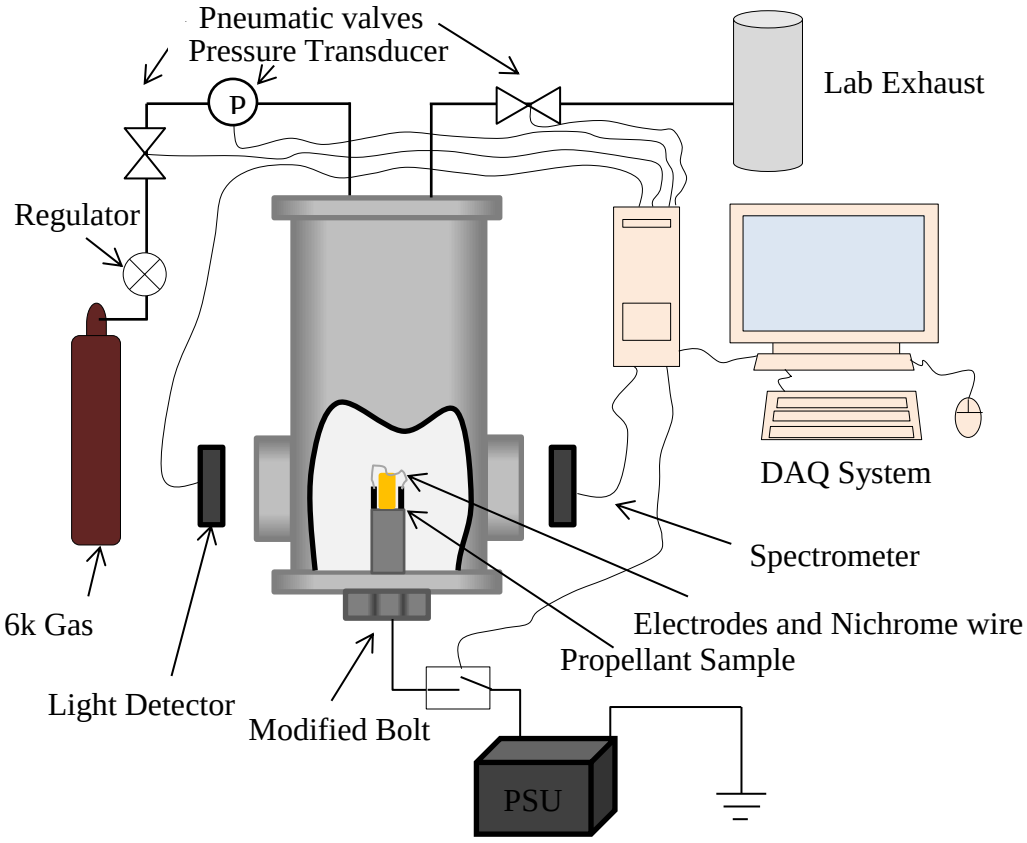

Figure 12: Strand bomb testing vessel with data acquisition computer.

As the propellant burns and gasifies, the pressure must rise inside the strand bomb due to the internal volume being constant. Pressure transducers placed along the inlet gas lines transmit this rise in pressure to a data acquisition system for recording. The rise in pressure due to the gasification of the propellant shows clearly defined starting and stopping points on a pressure-time trace. The time at which the pressure initially rises is taken to be the start of the burning process. Once the propellant burns completely, the pressure stops rising and at this point the time is again recorded and the test is over. With the known initial length of the propellant sample, and the time it took for the sample to burn, the burning rate can be calculated. The accuracy of this technique has been verified by both light trace and high-speed video. The pressure inside the strand bomb for a typical sample rises about 150 psi. This pressure rise is relatively small compared to the overall internal pressure of the strand bomb, and thus it is assumed that the burning rate is constant over this pressure range. Testing pressure for a given run is recorded as the average between the initial and final pressure within the strand bomb, which gives the assumption of constant burning rate more validity. Using the above procedure, multiple samples from the same formulation were burned at multiple test pressures, and the overall burning rate versus pressure profile was obtained. Figure 13 shows what the raw data looks like for a typical AP/HTPB propellant.

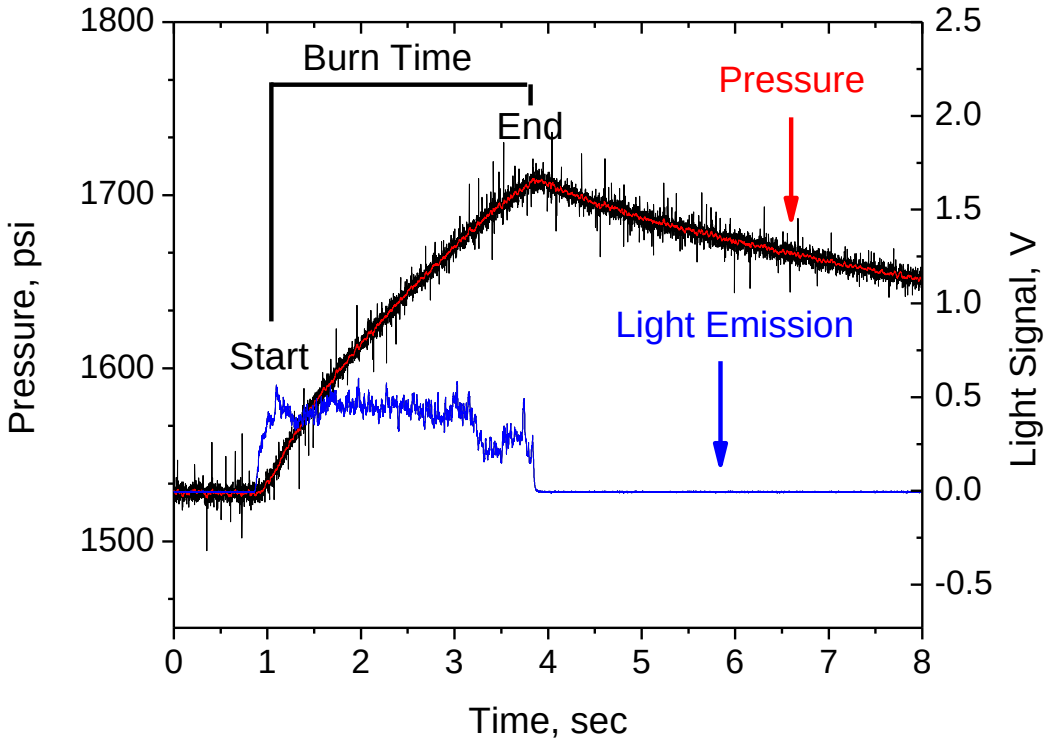

Figure 13: Typical pressure-time trace of a AP/HTPB propellant.

The black trace in Fig 13 indicates the pressure inside the strand bomb a few moments prior to ignition, during the event, and after ignition. Again the start of the test is indicated by a jump in pressure followed by a distinct halt in pressure rise. Under ideal conditions, the pressure would remain constant once the sample completes the burn, but due to various mixing and heat transfer effects, the pressure slowly decays immediately following the completion of the burn. This decay in pressure continues on until it reaches a thermodynamic steady state condition with the surroundings. This is of no consequence for burning rate measurements. The blue trace in Fig. 13 indicates the light

emitted through the combustion event, and it too displays clearly definable start and stop points. Spectral and high-speed video data are also collected during a typical experiment.

A range of monomodal, 20-to-200-µm AP was tested, however, it was expected that going much lower than 20-50 µm would result in diminishing returns since smaller AP sizes in HTPB are known to behave like a premixed system of AP and HTPB rather than as single AP particles [10]. A range of 70% to 85% AP by mass was also tested and correlated. Table 1 shows the detailed test matrix for this study.

Table 1: Detailed test matrix for the current study.

Formulation	**HTPB %**	**AP %**	**AP Diameter (µm)**	**Pressure Coefficient**	**Pressure Exponent**
1	15	85	206.7	0.0422	0.2851
2	20	80	206.7	0.0734	0.1972
3	23	77	206.7	0.0804	0.1698
4	25	75	206.7	0.1407	0.0834
5	30	70	206.7	0.1741	0.0320
6	20	80	138.0	0.1195	0.1760
7	20	80	72.7	0.0453	0.3549
8	20	80	45.7	0.0406	0.4152
9	20	80	23.4	0.0170	0.5469

CHAPTER IV

RESULTS AND DISCUSSION

Figure 14 shows the burning rate results for formulations 1 through 5. Data points are represented with symbols, and trend lines are added using the fit to Eqn. 1; the values for the empirical constants, a and n, are provided in Table 1.

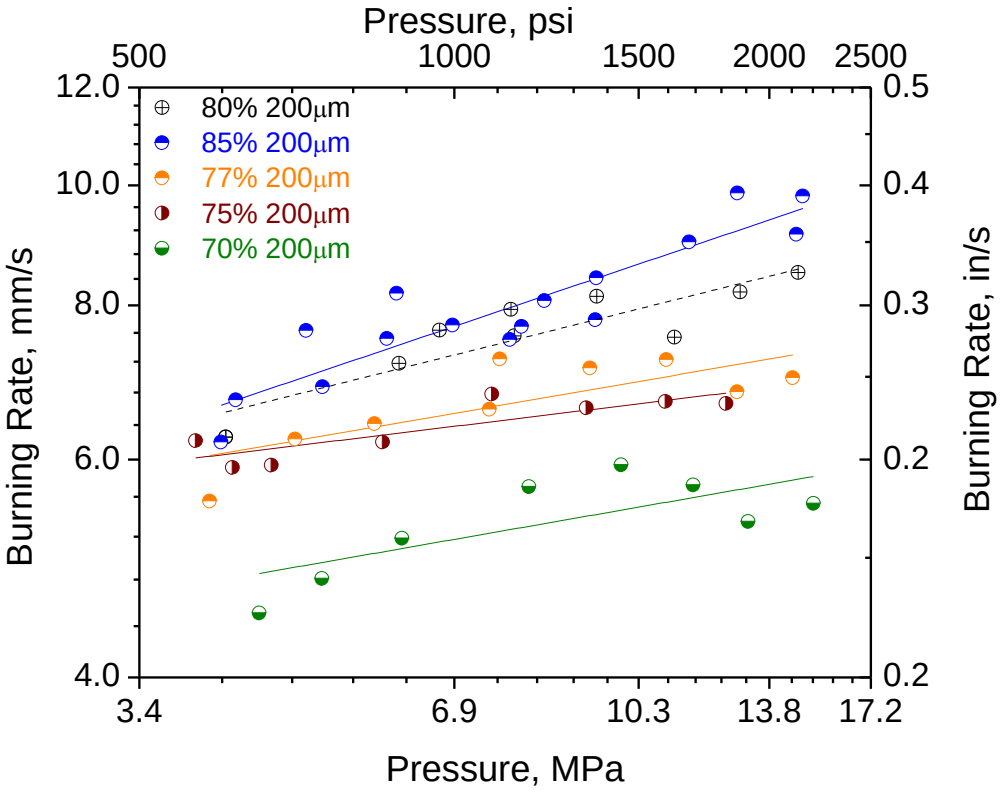

Figure 14: Baseline burning rate data for varying AP concentration and fixed AP particle size of 200 μm.

In Fig. 15, the burning rate of formulations 6 through 9 and also 2 are presented. This grouping of results was done to show the effects of changing the average AP particle diameter.

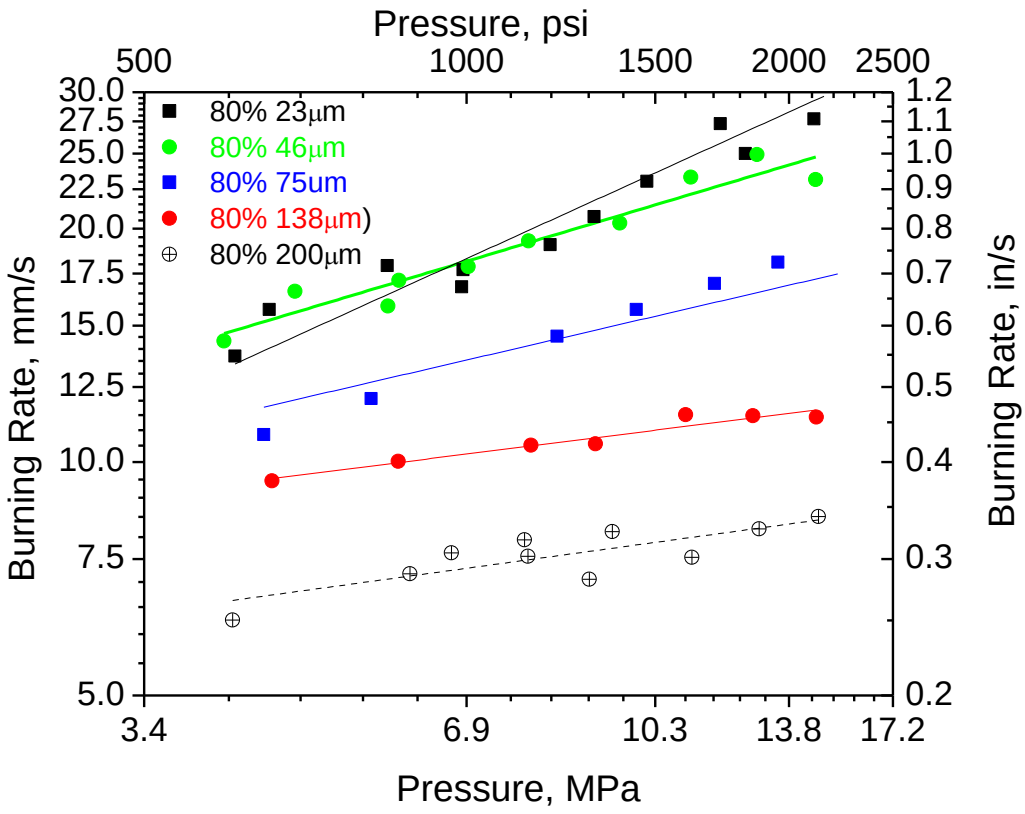

Figure 15: Baseline burning rate data for varying AP diameter and fixed concentration of 80% AP by mass.

From the data presented in Fig. 14, it was determined that the concentration of AP does indeed affect the burning rate, as expected. The data presented in Fig. 15 shows that decreasing the size of the AP leads to an increase in burning rate, and vice versa. However, going below a size of about 45 μm does not necessarily lend itself to an even higher burning rate. This diminishing effect was expected to happen at some relatively small oxidizer size because as the AP continues to decrease in size, eventually it will start to behave like a fully premixed system as mentioned earlier in the thesis; this seems occur around 40-20 μm.

A function in Microsoft Excel called "LINEST" was used for the first stage of the linear regression correlation of the burning rate data. The function inputs were based off of the linear trend lines of the data itself as opposed to simply entering the raw data from each set. The function was used two times to correlate both the pressure coefficient and pressure exponent as functions of AP diameter and concentration. This use of both parameters reflects actual trends in the data where it was seen that both fitting constants in Eqn. 1 vary with AP diameter and concentration, as shown functionally in Eqns. 2 and 3. Furthermore, by changing which data sets were included in the correlation, vast changes in the correlation's overall R-squared goodness-of-fit value was observed.

Rather than systematically trying every possible combination of function inputs, a plot was made which graphs the *n* and *a* constants from the power law (Eqn. 1) for each formulation against the independent variables. The independent variables are AP diameter and solids loading fraction. Figure 16 shows the plots of these constants as functions of the diameter and concentration of the AP in each size group. By doing this

step, the trends can be identified, and the outliers which might be throwing off the correlation can quickly be determined and removed from the list of inputs. As a result, the R-squared value was further improved from 0.90 to about 0.93. Later, a MATLAB script was used to further enhance the correlation, which improved the R-squared to the 0.968 that it is now.

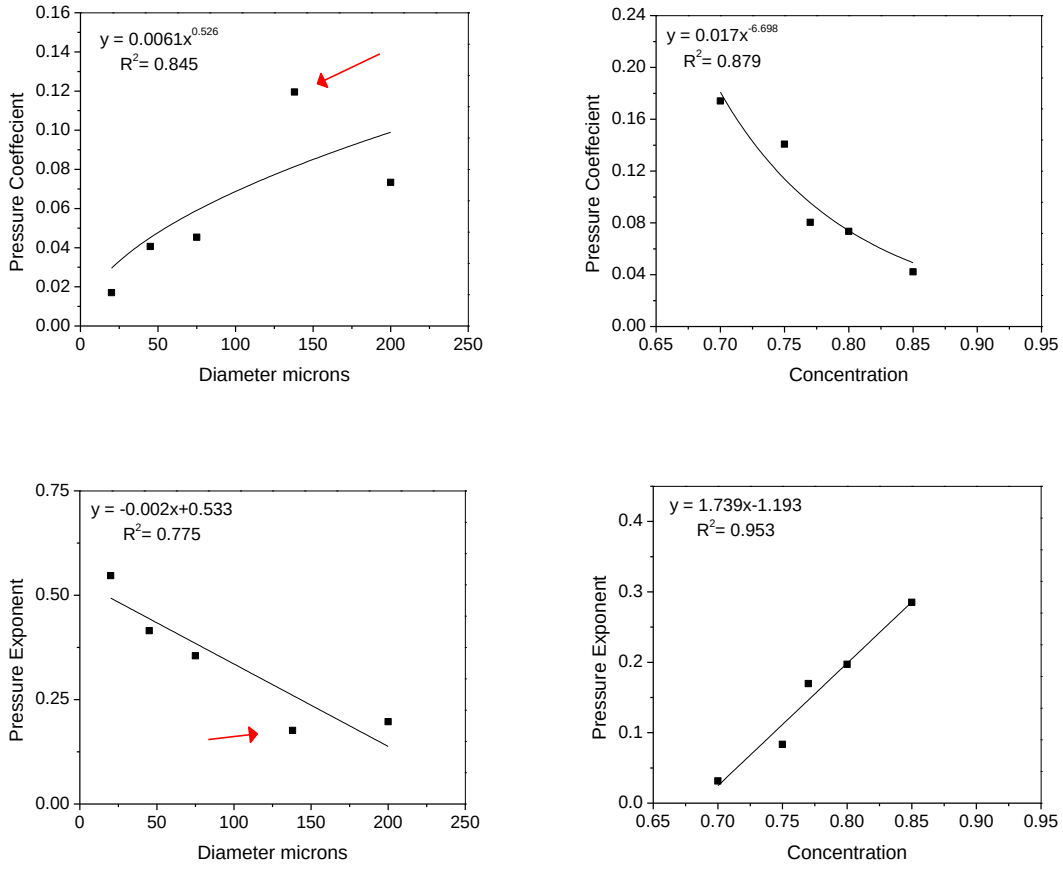

Figure 16 Pressure coefficient and exponent outlier determination for a) diameter versus pressure coefficient; b) concentration versus pressure coefficient; c) diameter versus pressure exponent; and d) concentration versus pressure exponent.

From Fig. 16, the only outlier seemed to be the 138-micron batch for both the pressure exponent and the coefficient. Interestingly, this batch also exhibited the most scatter in the first correlation. By removing the 138-micron results from the equation, the

correlation's accuracy was further improved. Using Fig. 16 as a starting point for the individual trends, a more-thorough master correction was sought.

To further improve the accuracy of the model, a short MATLAB script was used to finish fitting the correlation to the data. This allowed for the placement of more correlating constants than LINEST would allow, hence more accuracy. Equations 6 and 7 represent the final form of the correlation. Although this became the final form of the correlation, is it worth noting that numerous forms of the final correlation were attempted such as the following.

$$a = m_1 \boldsymbol{D}^{m_2+m_3\boldsymbol{C}} \boldsymbol{C}^{m_4+m_5\boldsymbol{D}} \tag{4}$$

$$n = m_6 + m_7 \boldsymbol{D}^{\boldsymbol{m_8}} + m_9 \boldsymbol{C}^{\boldsymbol{m_{10}}} \tag{5}$$

This procedure was done to ensure all suitable correlations were being considered. While some general forms did produce more accuracy, the increased accuracy was very small at the cost of immense complexity. Thus Eq. 6 and Eq.7 shown later were chosen for their simplicity and accuracy.

Furthermore, the nature of the MATLAB function "fitnlm" requires an initial guess for all the m constants before it can begin optimization. By getting the correlations for *a* and *n* close to their true values with LINEST, the MATLAB script was able to quickly converge on the final solution demonstrated later in Eq. 6 and Eq. 7. Data sets taken at TAMU by the author, data taken from Kohga [22], King [23], and Foster [24],

were all used in the final correlations optimization. Although not used to build the correlation, data taken from Bellec [28], Rochford [29], Hayakawa [30] and Frederick [31] were reviewed to observe how well the correlation predicts these datasets. Table 2 contains information regarding the testing conditions for each of these studies as well as formulation information.

Table 2: Formulation and testing information for all literature data sets utilized in the current study.

Reference	AP Details		Pressure Range		Binder Notes	Built Correlation	Matched w/ Correlation
	(%)	(μm)	(MPa)	(psia)			
King, 1979	73, 77	5, 20, 200	0.7-15.2	100-2200	HTPB, Carbon Black	Y	Y
Foster, 1982	75, 77.5, 80	12	0.7-20.7	100-3000	HTPB	Y	Y
Bellec, 1996	80	5, 90	0.6-98.5	80-14300	HTPB	N	Y
Rochford, 1999	75	17, 90	0.6-16.3	80-2400	HTPB	N	Y
Hayakawa 2000	73-80	15, 50	0.5-10.3	75-1500	HTPB, IPDI (5.75%), DOA (19.8%), MAPO (1.1%)	N	Y
Frederick and Osborn, 2000	66.7, 75, 80	16	1.7-13.8	250-2000	HTPB R-45M, IPDI (5.0%), DOA (25.5%), HX-752 (1.2%), Agerite White (2.0%)	N	Y
Kohga, 2011	55-80	4, 110	0.5-7.0	75-1000	HTPB, IPDI (8%)	Y	Y
Current Study	70-85	20-200	3.9-15.2	550-2200	HTPB R45-M, IPDI (8.74%)	Y	Y

Figure 17 is the graph of the master correlation as it attempts to correlate the concentration trends into one single empirical fit equation. For viewing purposes, individual trend lines of the data are removed, replacing them with the master correlation's prediction of the trend line. Equations 6 and 7 are the correlations used to make the dotted fit lines in Fig. 17 through Fig. 29. Units for this correlation are psi for pressure, microns for diameter, and (0.XX) for concentration where inputs for XX are valid from 65 to 85 corresponding to 65% and 85% AP by mass. The model is only valid for an average AP particle size of 4 to 200 microns.

$$BR = aP^n \tag{1}$$

$$a = 0.438\boldsymbol{D}^{-0.942+1.034\boldsymbol{C}}\boldsymbol{C}^{14.702-0.045\boldsymbol{D}} \tag{6}$$

$$n = 1.736 - 0.002\boldsymbol{D} - 1.397\boldsymbol{C} \tag{7}$$

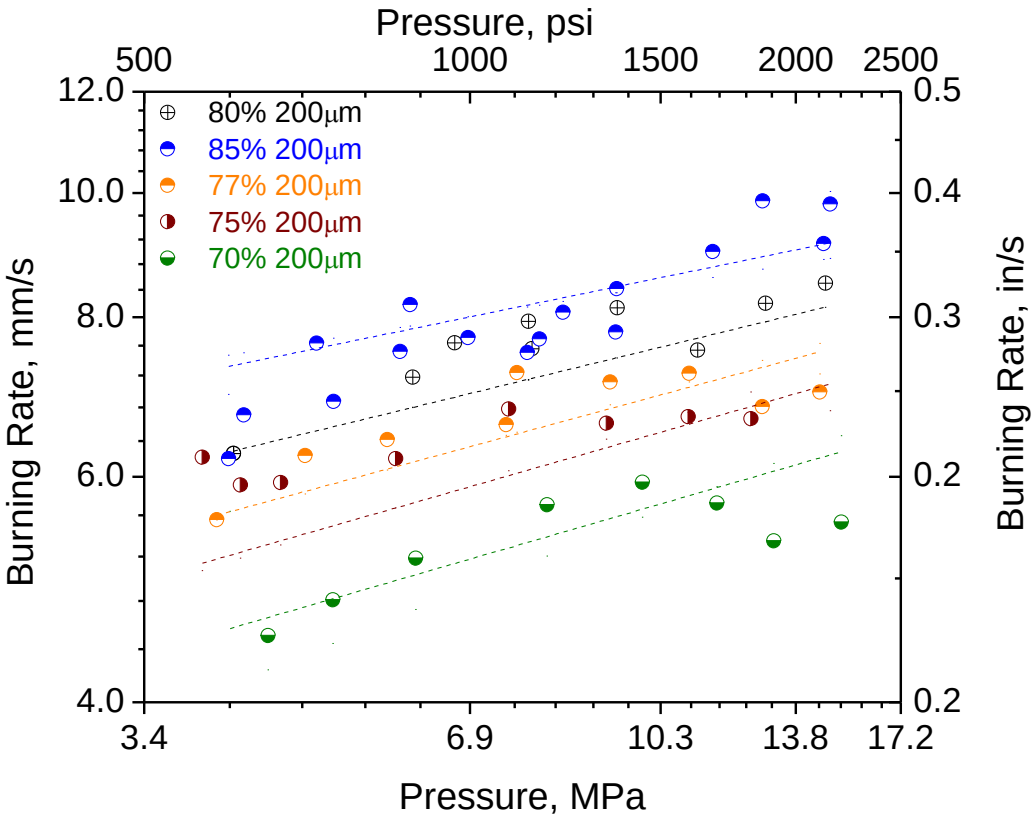

Figure 17 Comparison of the individual burning rate data for the 200-μm AP cases with the results of the master empirical correlation of Eqns. 6-7 (dashed lines).

As is shown in Fig. 17, the correlation does a good job of matching the data. It also captures the general effect that concentration of AP has. Generally, as concentration is raised, burning rate raises and vice versa. In Fig. 18, the effects of changing the average AP particle diameter are also well predicted with the correlation.

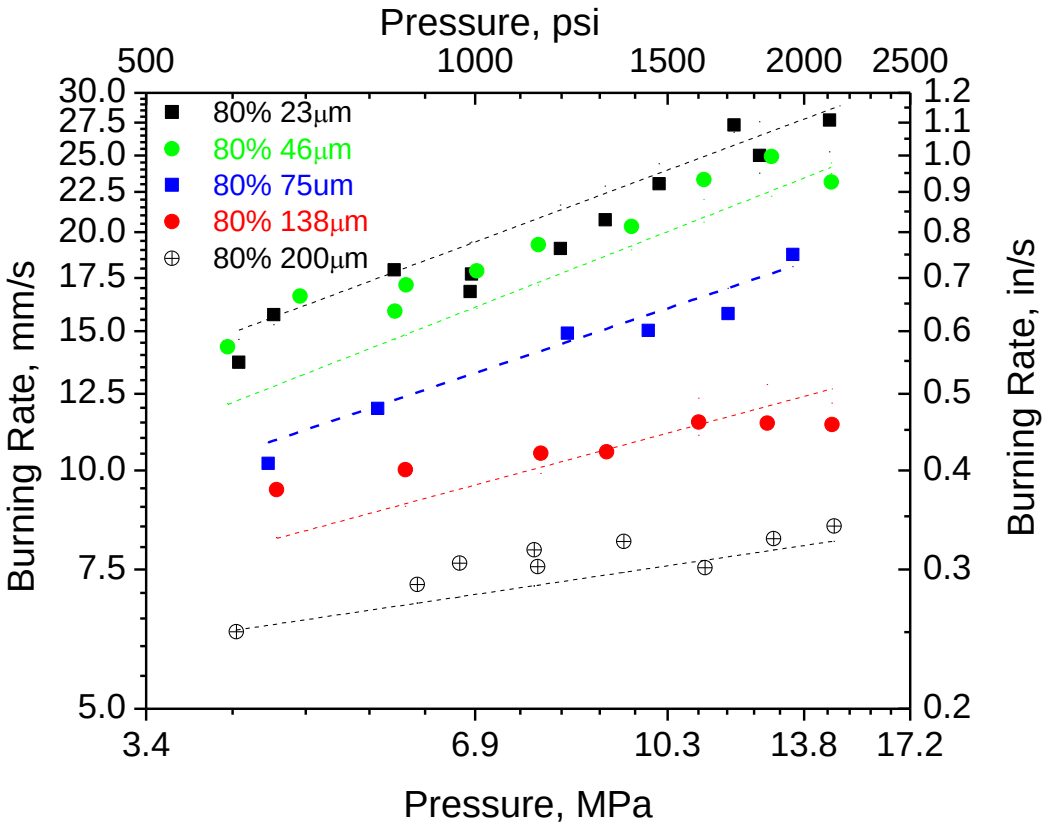

Figure 18: Comparison of the individual burning rate data for the 80% AP cases with the results of the master empirical correlation of Eqns.6-7 (dashed lines).

The correlation is able to predict the burning rate data in which the average AP particle size is changing with great accuracy. Again, it also captures the general effect that changing the average AP particle size has on burning rate. In general, decreasing particle size increases burning rate. Figure 19 gives the scatter plot for the formulations in which AP concentration was changed.

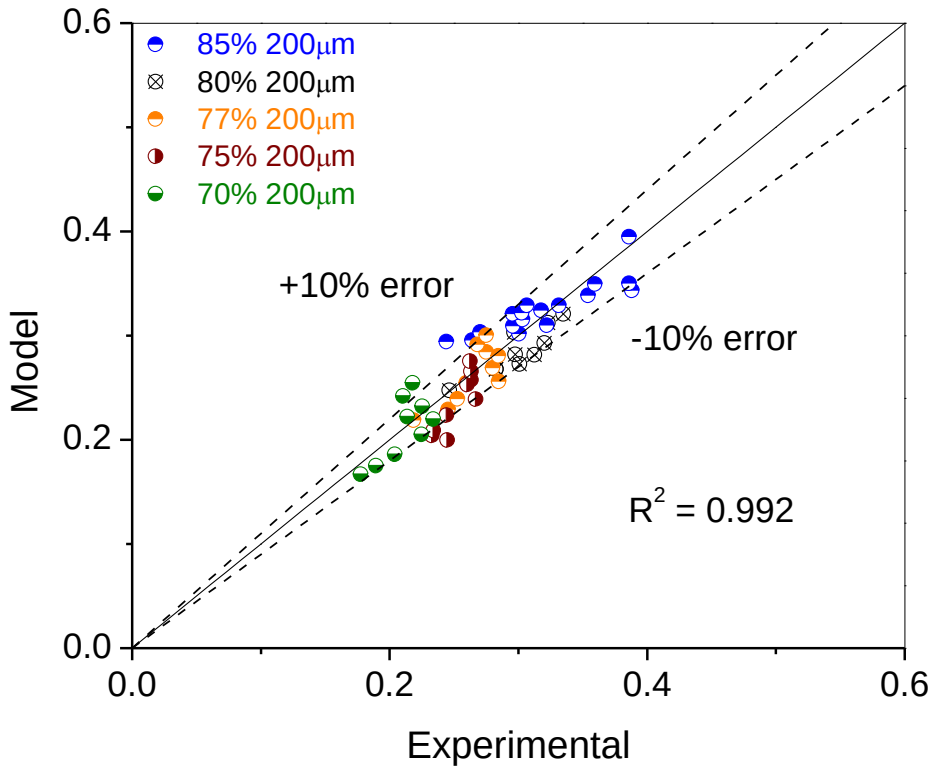

Figure 19: Scatter plot of the master correlation of Eqns. 6-7 for TAMU formulations where AP concentration is varied.

Figure 19 plots the model's prediction of each individual data point against the experimental data point. Along the horizontal is a line with a slope equal to one which represents a perfect fit between the data and the correlation. Ideally, every point would fall right on top of this line, which translates to a high R-squared value, but when they do not extra dash lines are added which indicate the error in the correlation in terms of a percentage. The vast majority of the correlated data falls within 10% of the experimental data, while the average error is around 7.3%.

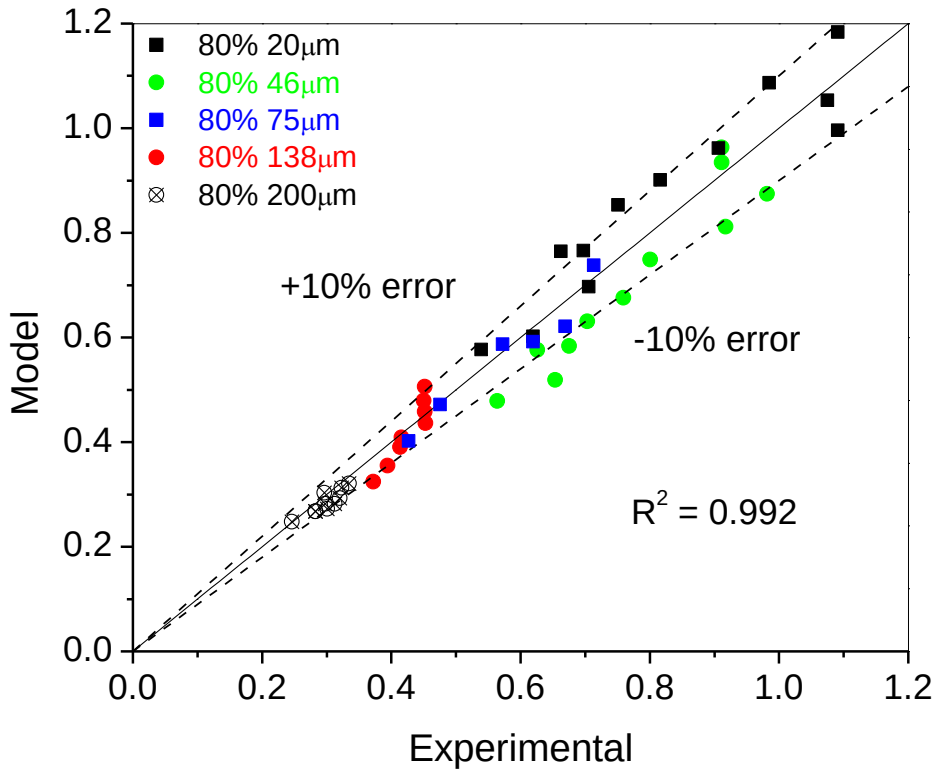

Figure 20: Scatter plot of the master correlation of Eqns. 6-7 for TAMU formulations where average AP particle size is varied.

Figure 20 gives the scatter plot for the formulations in which average AP particle diameter was changed. Like before, the correlation fits almost all the data within 10%, while the average error is again 7.3%. The goal was to get above an R^2 value of 0.9 or better, and the correlation actually has an R^2 of 0.992 which is impressive considering the simplicity of the model. Furthermore, the fact that the burning rate as a function of pressure, diameter, and concentration can be correlated with such a simple technique has implications for future studies within itself.

For further validation, the model was also used to predict burning rate data for the authors previously mentioned in the background section and listed in Table 2. For this next graph, Fig 21, the data come from Kohga [22] and cover a wide range of concentration while keeping the size of the AP at 110 microns.

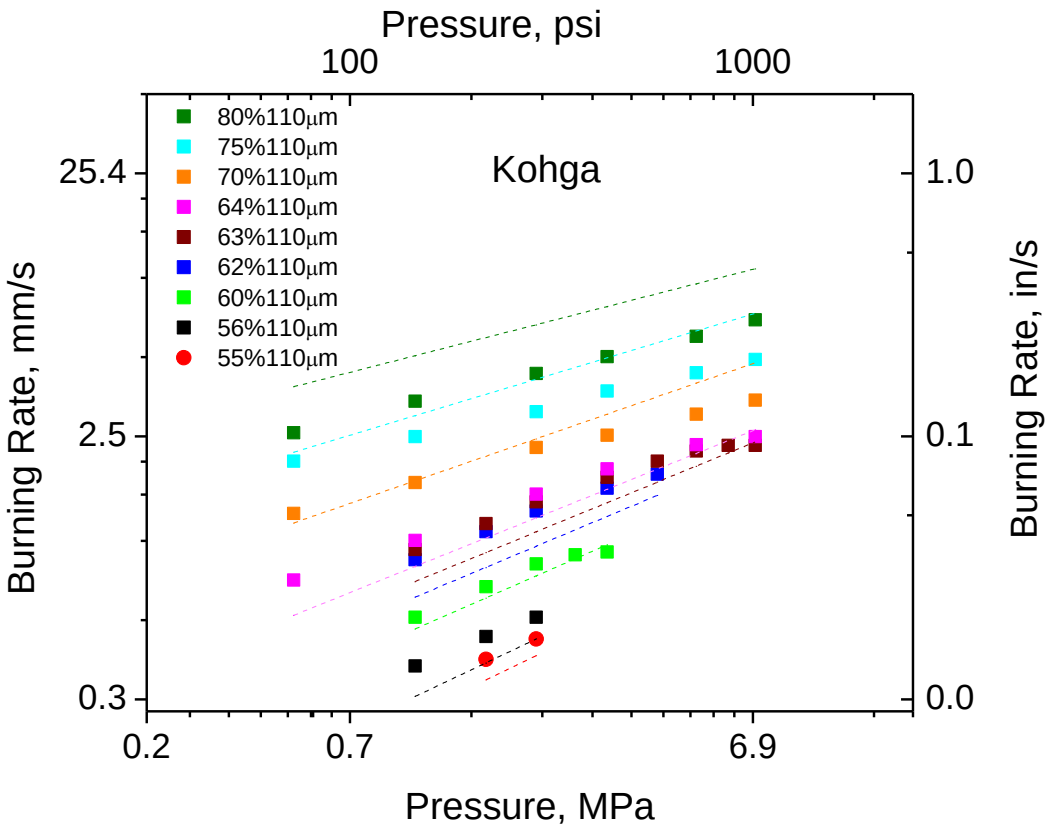

Figure 21: AP/HTPB 110 micron baseline burning rate data while varying AP concentration taken from Kohga **[22]**.

In Fig. 21 one can observe that the concentration effect at this particle size is exaggerated by the correlation at low concentrations and over estimated at higher concentrations. While the individual slopes of each trend line are good, their vertical

placement on the graph can be improved. In Fig. 22, the same data and correlation are repeated except using 4 microns for the average AP particle size.

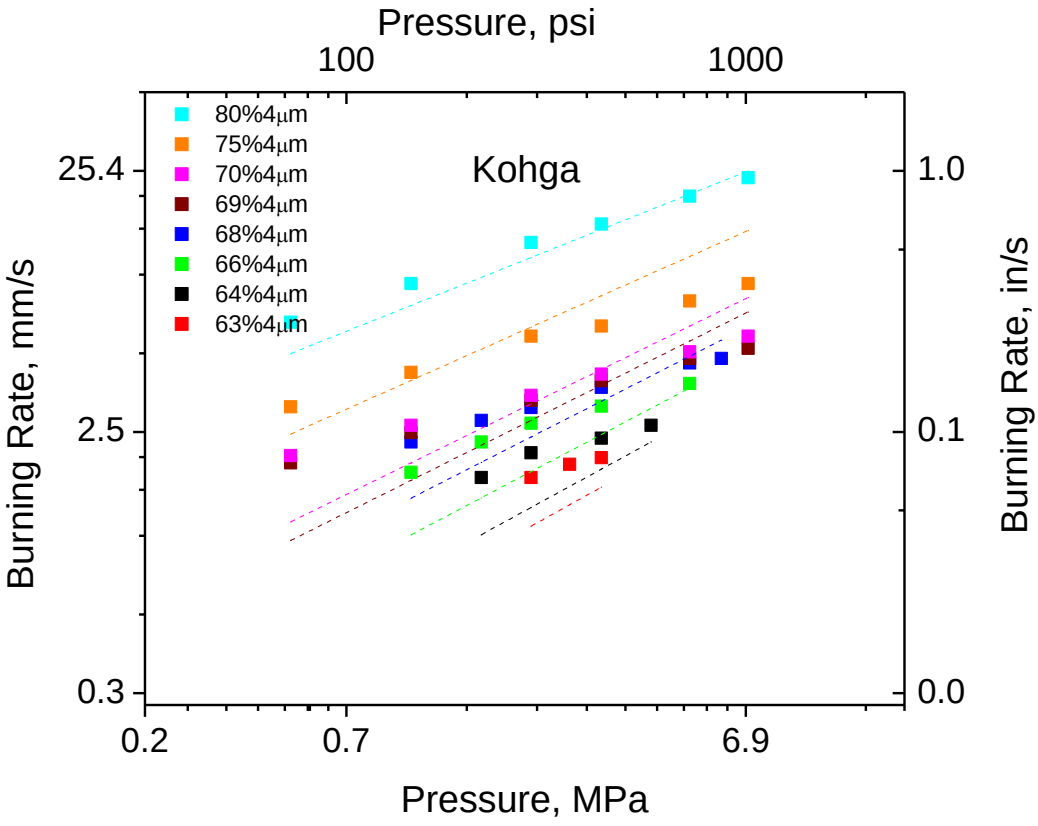

Figure 22: AP/HTPB 4 micron baseline burning rate data while varying AP concentration taken from Kohga [22].

While the correlation continues to capture the general effect of concentration, it is slightly under predicting the placement of the trend line at lower burning rates, much like before. There is some discrepancy in the slope for the intermediate batches as well. These formulations also contain AP sizes that lie on the edge of the correlations range so this to could be why.

Figure 23 contains data taken from King, and it too is correlated with the master correlation Eq. 6. King, unlike Kohga, did not explore mixture with AP concentrations below 73% and instead kept his propellants confined to the 73-to-77% AP concentration range. He also tested three sizes of AP instead of two. It is also worth noting that King used a small amount of carbon black in his binders which is typically used as an opacifier to absorb radiation near the fuel surface. This is believed to have a nearly negligible effect on burning rate, and the results still agree rather well with the predictions of the master correlation.

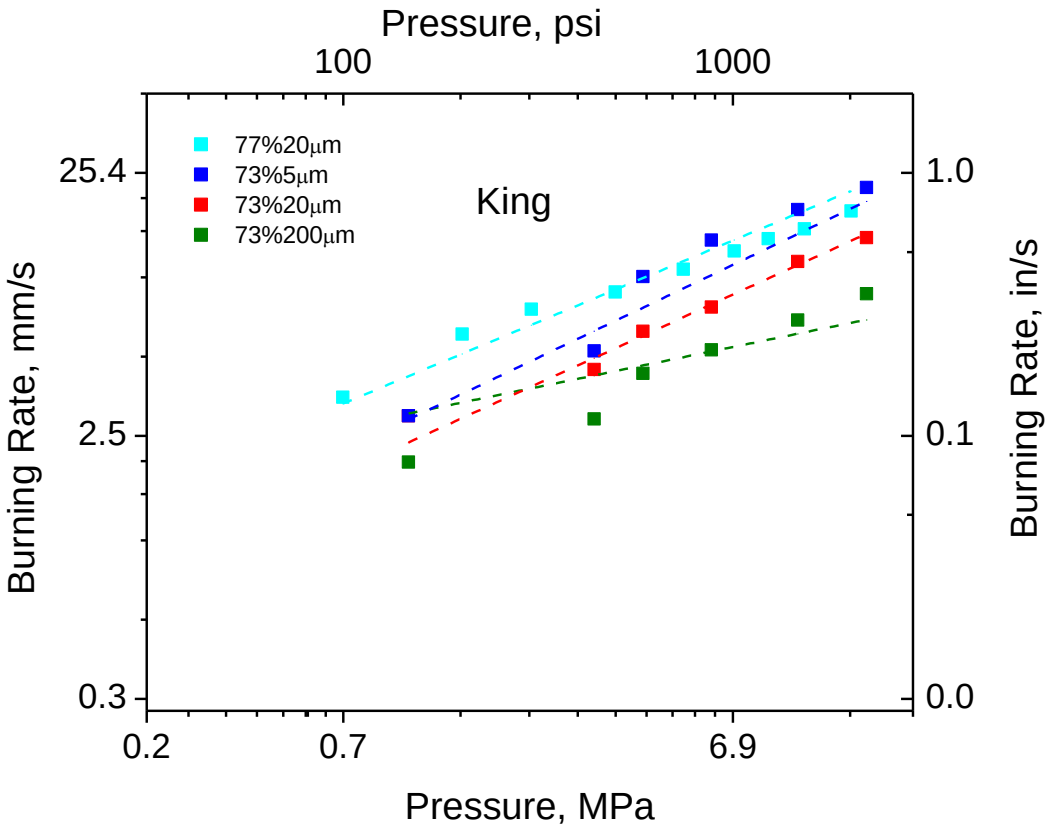

Figure 23: AP/HTPB baseline burning rate data with varying AP concentration and size taken from King **[23]**.

The correlation does a much better job at predicting the data as pertaining to King's data set. Only the lower 200-micron formulation shows slight deviation. Lastly is Foster's baseline burning rate data set displayed and correlated in Fig. 24. All of his formulations contained 12-micron AP, which was not tested previously by others and fills the gap between the 5- and 10-micron sizes.

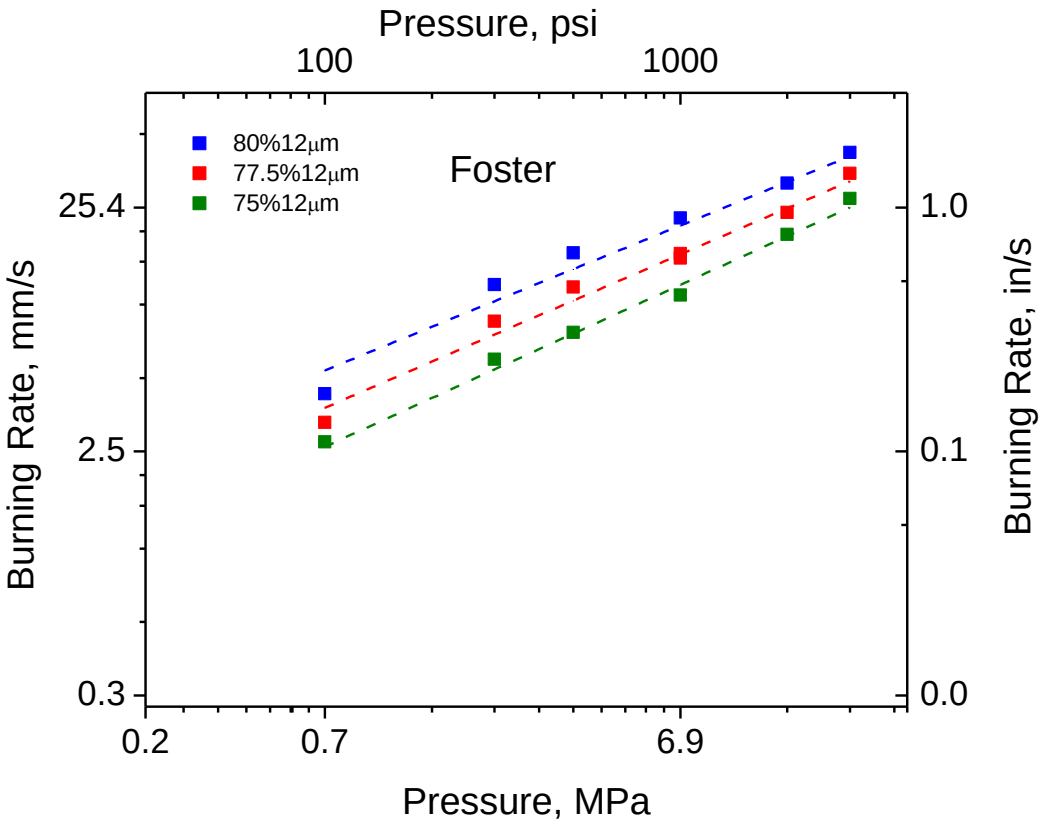

Figure 24: AP/HTPB baseline burning rate data while varying AP concentration taken from Foster **[24]**.

More than any other mixture, the correlation excels in predicting Foster's data and does so without any appreciable error. Next, the scatter plot of all the data is presented in Fig. 25.

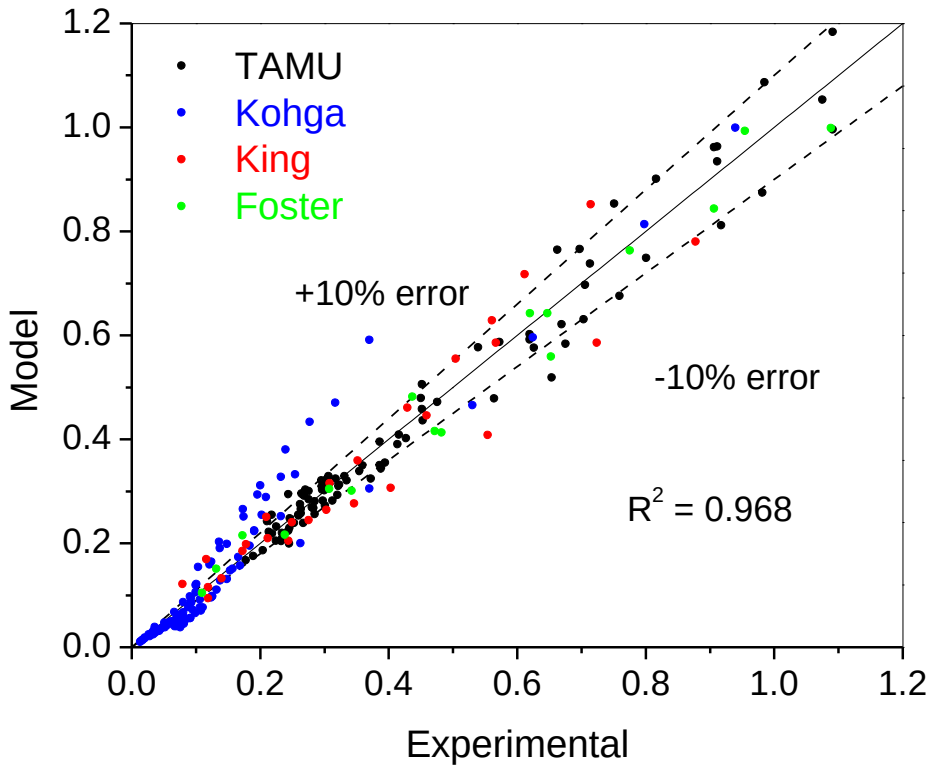

Figure 25: Overall scatter plot of correlated data from TAMU, Kohga, King, and Foster.

Ultimately, the model produces an overall R-squared value of 0.968, which is slightly lower than the one it produced when only taking into account data taken from TAMU. Nonetheless, the accuracy is substantial considering the ease of which the correlation was built. From the overall scatter plot, only Kohga's intermediate propellants deviate far beyond the 10% mark.

The next few figures focus on the remaining data sets as listed in Table 2. Although they were not included in the master correlation's development, it can still be useful to apply the correlation to these data sets. In Fig. 26 data taken from Bellec [28] are plotted against the correlation's prediction.

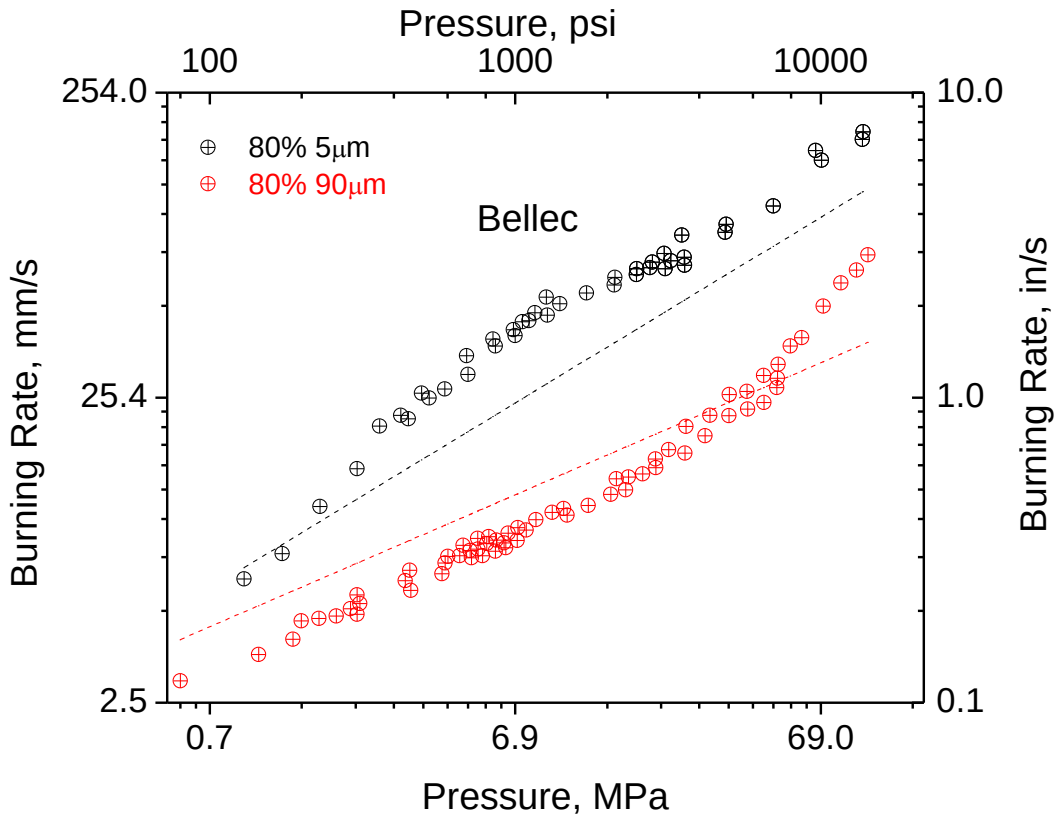

Figure 26: AP/HTPB baseline data take from Bellec.

Again the model demonstrates its ability to match the basic trends seen in the data. A key note is that Bellec did not mention the curative he used for his propellants. This detail can be causing some discrepancies because different curatives have been seen

in past studies to bring about minor changes in burning rate; but despite this, the correlation aligns well with the experimentally observed particle size effect. Bellec's data also spans a huge pressure range that encumpases the exponent break seen in APCP's which the correlation is not yet equipped to handle. This is seen in the latter half of the figure where the data and correlation trend line cross paths.

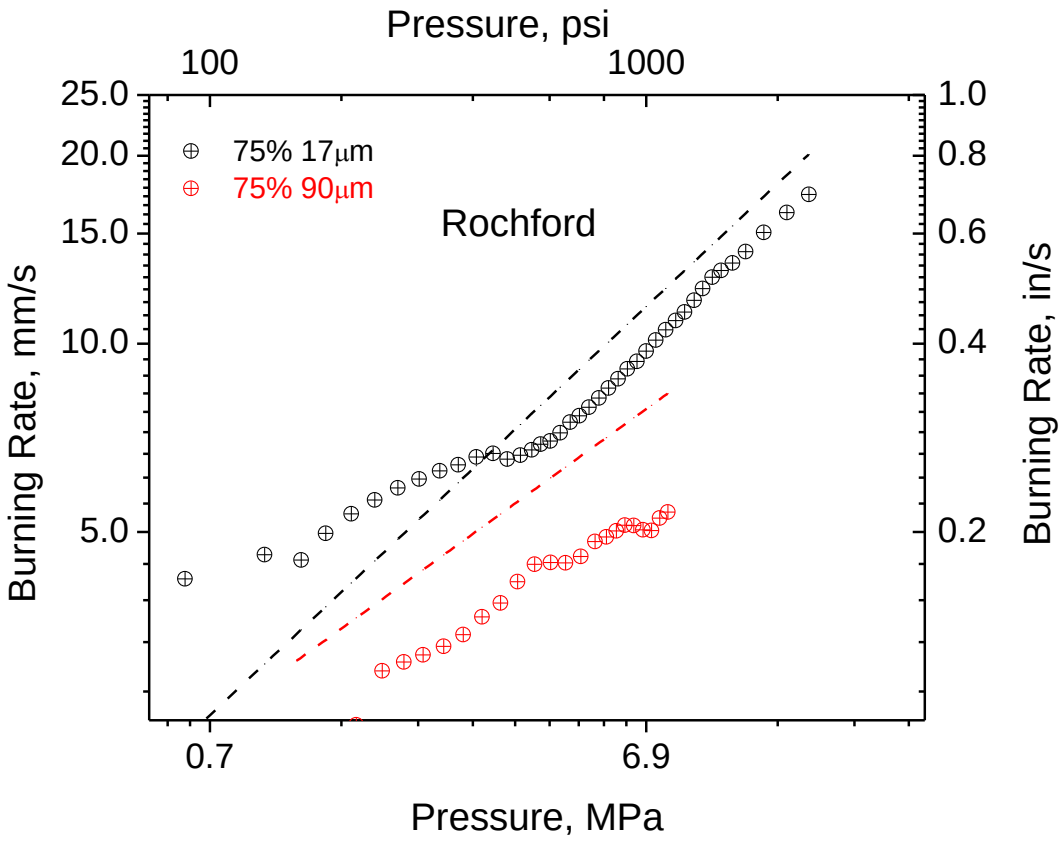

Figure 27: AP/HTPB baseline data taken from Rochford.

Figure 27 represents data taken from Rochford [29]. The correlation, represented by the dashed lines, aligns better in the higher-pressure regime (>4 MPa) than the lower-

pressure one (<4 MPa). Rochford in his experiment measured burning rate through the use of a technique called the ultrasonic pulse echo technique. His strand burner has a small internal volume not that much bigger than the propellant samples themselves. This rather small internal volume makes the pressure rise seen inside the strand bomb very great for a single test, and with incremental burning rate measurements a single sample can be used to obtain the entire burning rate profile. This technique has been known to be less accurate when measuring burning rates, especially at lower pressure, and could be causing some discrepancy between the correlation and the data.

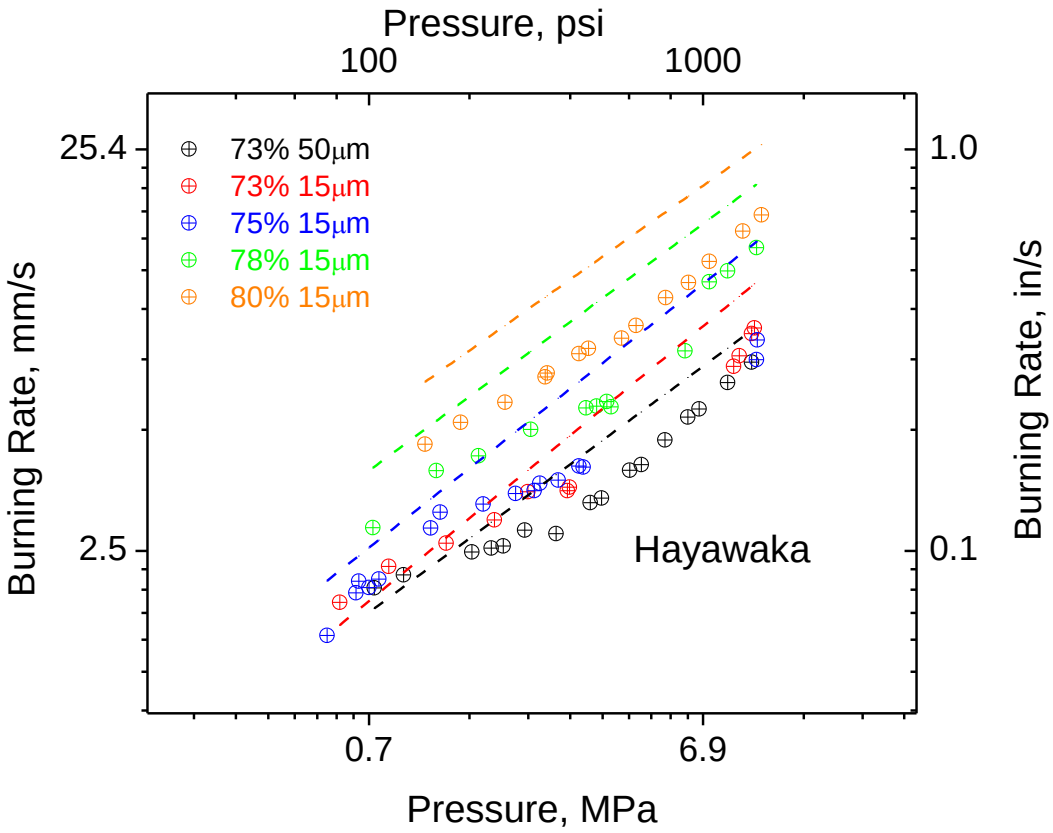

Figure 28: AP/HTPB w/ DOA burning rate data taken from Hayawaka.

Figure 28 represents data taken from Hayawaka. In his formulation, Hayawaka used a large amount of plasticizer, namely DOA. Hayawaka used approximately 20% DOA. As the figure shows, the correlation generally over predicts the burning rate for all formulations. This difference is not unexpected as it is known that high amounts plasticizer decrease the burning rate compared to pure baseline formulations with just HTPB. In general, although the trends align well and if these formulations were true baselines they most likely would have aligned better and would have been included in the master correlation's development.

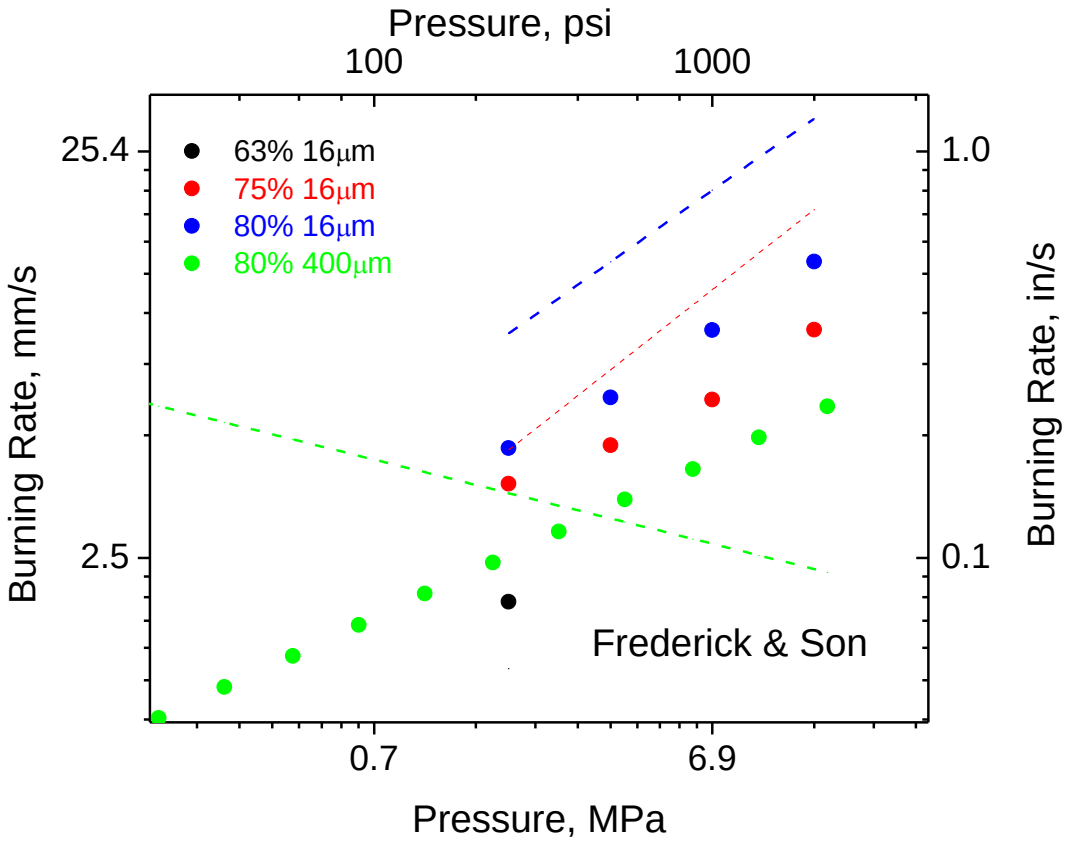

Figure 29: AP/HTPB w/ DOA propellant burning rates with various size and concentration of AP taken from Frederick **[31]**.

Figure 29 displays data take from Frederick [31] and covers a wide range of both average AP particle size and AP concentration. He too used a large amount of DOA which can also explain why the model generally over predicts the measured burning rates. Notice for the 400-micron formulation the correlation actually predicts a trend line with a negative slope. This is because 400-micron result lies outside the correlation's acceptable range. As is shown in Fig. 30, there exists an acceptable range of inputs for the correlation where if users use inputs beyond this range the correlations breaks down.

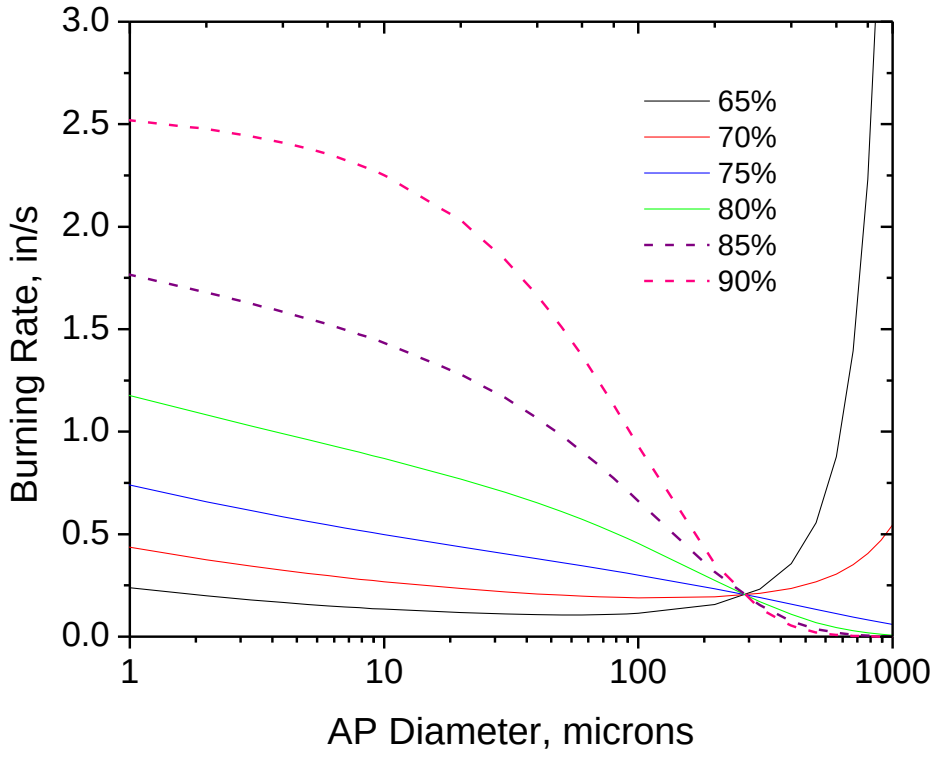

Figure 30: TAMU correlations predicted burning rate as a function of AP diameter and concentration at a pressure of 1000 psia.

Notice in Fig. 30 at around 300 microns, all predictions of the correlation for various formulations converge to a single point. After this point, the trends that were present before reverse themselves. This crossover is why the 400-micron batch produced a negative slope, which is not what experimental results show is the case. While the model is not complete, it still offers good results when properly used for AP sizes near and below 200 microns.

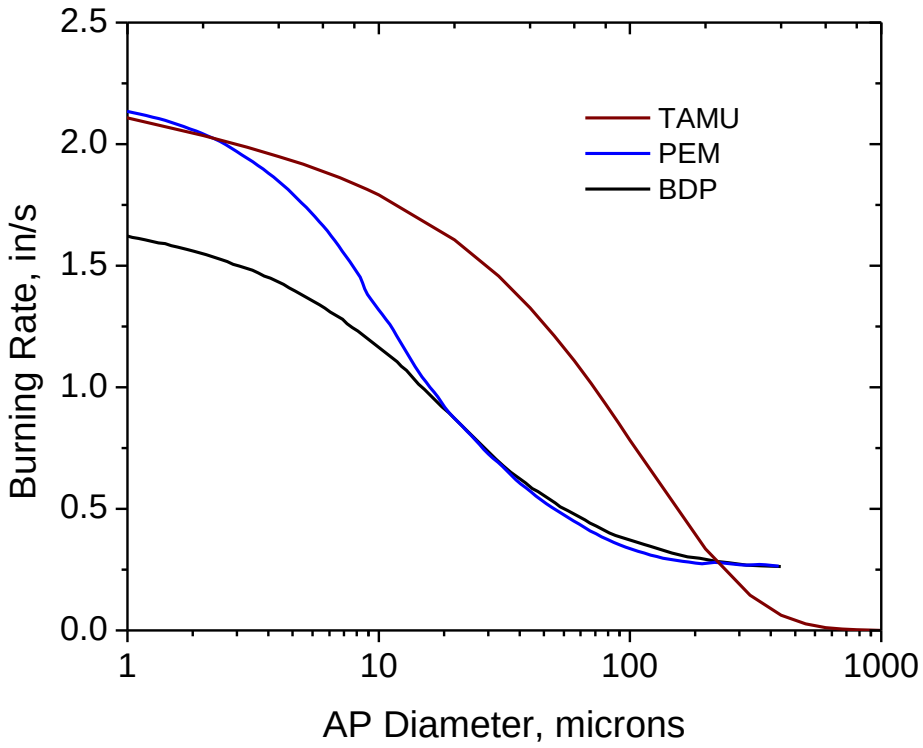

Figure 31: Predicted burning rates versus AP diameter for the DBP, PEM, and TAMU models/correlations.

Figure 31 represents the burning rate prediction of the historical BDP and PEM models alongside the TAMU correlation. Plotted with AP diameter on the x axis, the correlation aligns well with the other models when AP diameter is small. During the intermediate region, it deviates and later realigns at higher AP diameter. Again the correlations ability to re-create the general trends of well-established historical models shows its promise. Note however, that the theoretical models were created based of an

87.5% AP formulation, which lies outside the tested range of the correlation, and at a pressure of 1000 psia. At lower AP concentrations, where the TAMU correlation was developed, the models would likely agree more closely.

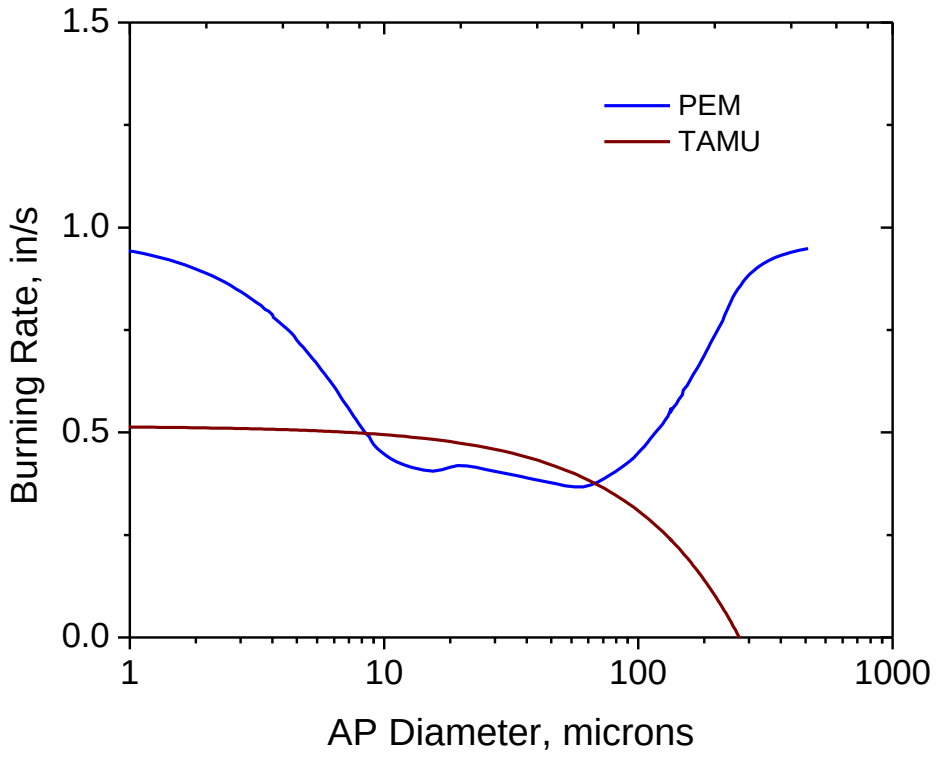

Figure 32: Comparison of PEM and TAMU's prediction of pressure exponent as a function of AP diameter. 87.4% AP at 1000 psia.

In Fig. 32, a comparison of the PEM and TAMU correlations is drawn as it pertains to the pressure exponent as a function of AP diameter. In the region of interest, between roughly between 10 and 200 microns, the two agree rather well but with some discrepancy. Outside this region they do not agree, and the TAMU correlation's

prediction of the pressure exponent quickly falls off and even becomes negative when going past 200 microns. Again, outside the acceptable range as detailed in Eq. 6, this correlation should not be considered.

CHAPTER VI

FUTURE WORKS

In the future it is the author's wish to include more formulations and more data for each formulation to help with correlating and accuracy. This correlation represents the first step in modeling from a practical standpoint, and as such, there exists a huge potential to add in effects of additive formulations such as those containing *in-situ* TiO_2 or Fe_2O_3. In addition to the AP size and concentration, the correlation would have to include terms for the additive's size and concentration and also the additive's relative catalytic effect. This technique's ease of applicability makes it a valuable tool that researchers can use to correlate trends in data not just for APCP baseline burning rates but for perhaps an even wider range of applications. In addition, future studies should include the effects of AP size distribution and the existence of bimodal and even trimodal size distributions as well.

AP/HTPB composite propellants have also exhibited what's called an "exponent jump" which happens at a characteristic a pressure that typically lies above at least 14 MPa (2,000 psi) [28]. Decomposition studies have also shown that AP reacts differently at this same pressure [29].

The AP takes a jump in burning rate around 35 MPa (5,000 psi) and when laced within a binder, such as in a propellant, the contribution of the AP burning rate to the total burning rate becomes dominant [30]. Researchers at the author's laboratory have also seen this behavior first hand in their own testing, although no publications have been made. When plotted on a log-log plot, the sudden change in slope results in a jump of the pressure exponent, which is where the term "exponent jump" derives.

In Fig. 33, the burning rates of aluminized AP/HTPB propellants are shown as adopted from Atwood. The various formulations contain different AP concentrations and sizes, different concentrations of micro-aluminum, and some contain Fe_2O_3 burning rate catalyst. Again the same exponent jump is seen, but the characteristic pressure ranges from 18-22 MPa (2.6-3.2 ksi). An interesting observation is that the catalyst has a great effect on burning rate prior to the exponent jump, but little effect afterwards. It also shifts the characteristic pressure itself.

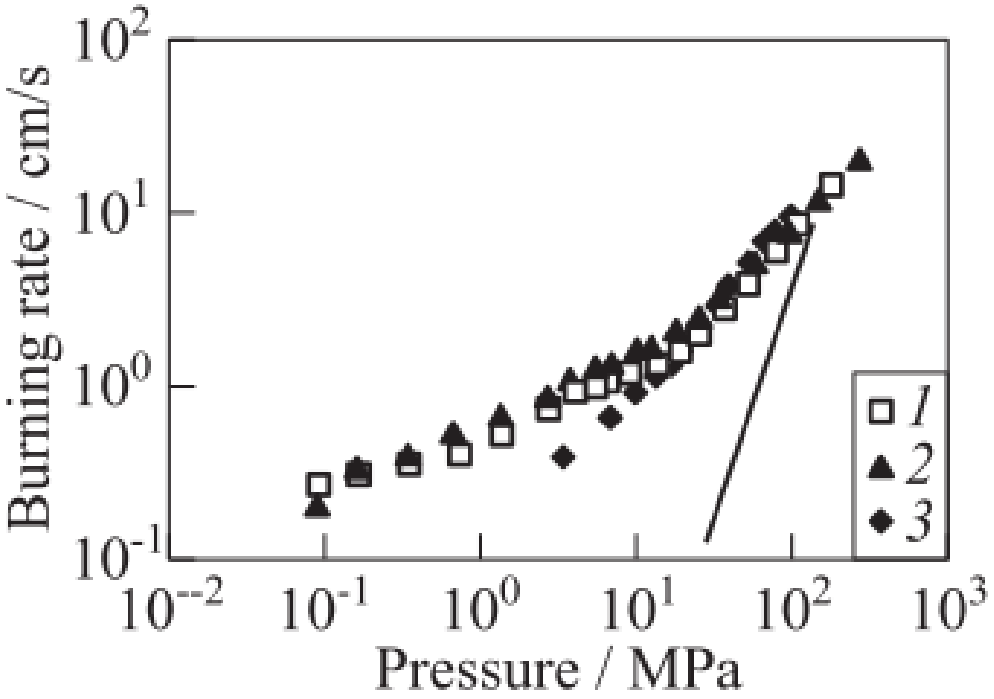

Figure 33: Burning behavior of composite AP/HTPB/AL propellants, taken directly from Atwood **[28]**

There has been many attempts at explaining why AP exhibits this type of behavior [31] [10].The current most-support theory proposed by Irwin suggests that at high pressure mechanical stress on the AP is leading to surface break-up, increased burning area, and as a result the increase in burning rate [32]. Whatever is creating this stress, whether it is hydrostatic, temperature gradient, crystal phase transition, etc., it is not fully understand and has not been determined.

In any case, baseline burning rate trends should be correlated out beyond this characteristic pressure. Things like the characteristic pressure itself, as a function of AP particle diameter and concentration, and the post-5,000 psi trend lines themselves could all easily be characterized.

Furthermore, APCP's exhibit sensitivity when it comes to initial temperature as seen in previous studies at the author's laboratory [33]. This same trend has also been seen by others [10]. In general, by heating the propellant before ignition, the propellants demonstrated an increase in burning rate and when cooled down, the burning rate decreased. Figure 34 is adopted from Demko [33] and depicts these temperature-related trends.

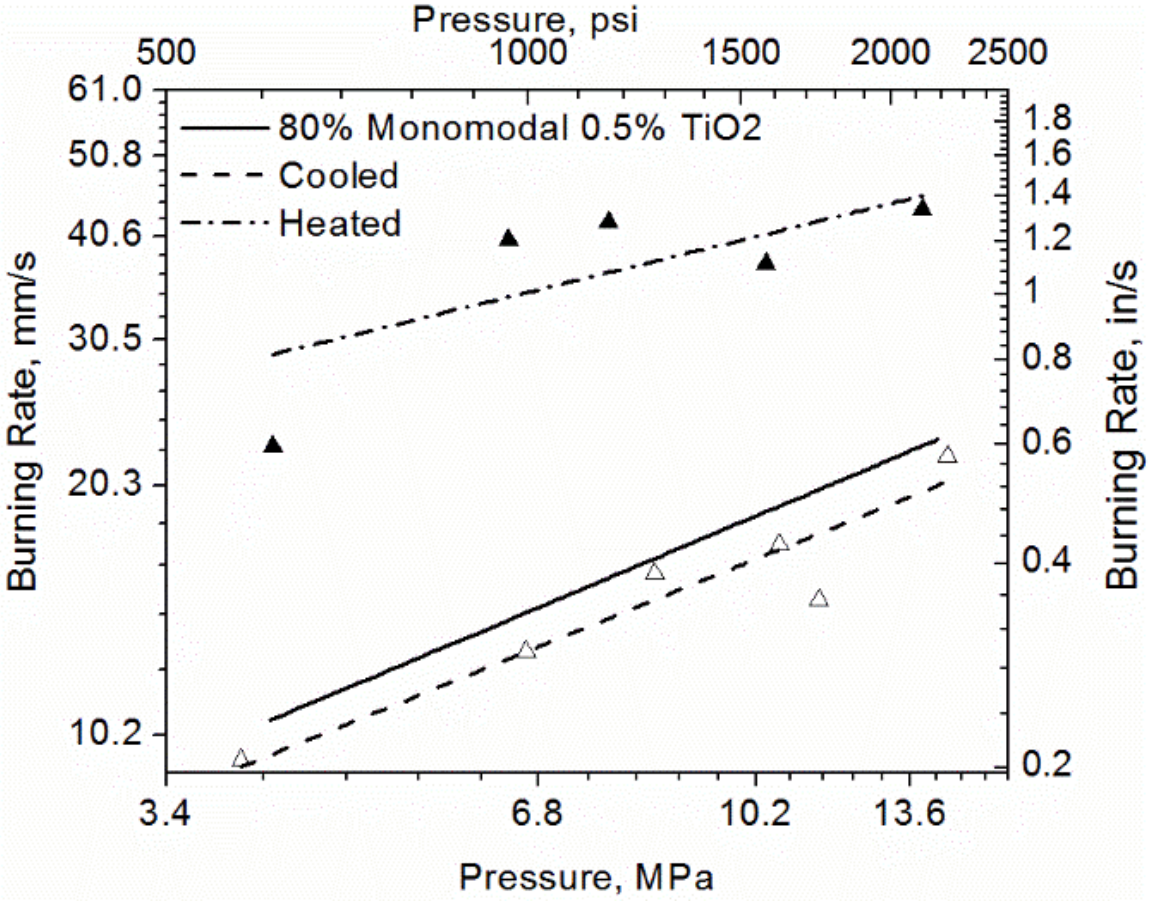

Figure 34: Initial Temperature Effects on AP/HTPB based composite propellant burning rates. **[33]**

A temperature term in both the pressure exponent and coefficient could easily be introduced to include its effect in the model. However, extensive testing for every formulation at both high and low temperatures would need to be performed.

It would also be interesting to see if the pre-5,000-psi trends maintain themselves into the post-5,000-psi regions. Would the difference between a 200-μm propellant and a 20-μm propellant become narrower due to the cracking, or perhaps even negligible? While there have been tests at this pressure, there still exists a lack of extensive data which are needed for adequate characterization from a statistical standpoint.

Lastly, the BDP and PEM models should be accurately applied towards making an all-inclusive burning rate database that can be used to compare one model's prediction with the others as well as this study's correlation.

CHAPTER VII

CONCLUSION

In this research, the effects of AP particle size distribution and concentration within an HTPB binder were studied as it pertains to burning rate. Not surprisingly, the effect of reducing the AP particle size produced the most drastic change in burning rate. Changing the concentration, and therefore the equivalence ratio, also produced an effect in the burning rate, although much smaller than that due to AP size. Control over the burning rate is crucial in rockets for many reasons. Understanding how AP size and concentration affect the burning rate gives engineers the information they need to build safe, stable rockets that operate efficiently as they are intended throughout their entire mission. Providing a simple algebraic correlation makes it easy to quickly determine burning rate for AP/HTPB baseline formulations. Also, intermediate regions on the burning rate curve where data do not exist can be backed out by interpolation. During the fabrication of these propellants, going lower than 75% AP by mass started becoming a problem due to settling effects. It was not without great difficulty that these propellants were made. For most applications, 80% solids loading and above is preferred. However, on the higher end of AP concentration the brittleness of the propellant in cured form then starts becoming a problem for implementation purposes as well as safety.

While baseline formulations without additives are not widely used, they are important to understand as a starting point and for comparison to more-sophisticated models of the burning process. In the future, researchers should strive to extend this type

of statistical correlation to include the effects of advanced nano-scale additives such as *in-situ* titania, *in-situ* iron oxide, or *in-situ* aluminum. Initial propellant temperature also has an effect, and the exponent jump needs to be considered as well for applications that intend to operate above the propellant's characteristic pressure.

While the inclusion of these effects might complicate the algebraic form of the master correlation, plugging known concentrations of materials into a large exponential equation is still much easier than using computers to iteratively solve kinetic equations while balancing heat and mass flux conservation laws. Until deeper knowledge in these areas is developed, correlating APCP burning rate trends from a statistical point of view offers an alternative to theoretical modeling.

REFERENCES

[1] B. Dunbar, "Space Shuttle Solid Rocket Boosters," 5 March 2006. [Online]. Available: https://www.nasa.gov/returntoflight/system/system_SRB.html. [Accessed 05 June 2016].

[2] A. T. (ATK), "ATK Space Propulsion Products Catalog p. 30," May 2008. [Online]. Available: http://www.ltas-vis.ulg.ac.be/cmsms/uploads/File/DataSheetSolidATK.pdf. [Accessed 5 June 2016].

[3] G. P. Sutton, "Rocket Propulsion Elements: An Introduction to the Engineering of Rockets", 7th ed., New York: Wiley, 1986, p. 455.

[4] G. P. Sutton, "Rocket Propulsion Elements: An Introduction to the Engineering of Rockets", 7th ed., New York: Wiley, 1986, p. 428.

[5] E. K. Bastress, "Modification of the Burning Rates of Ammonium Perchlorate Solid Propellants by Particle Size Control," Thesis, Aeronautical Engineering, Princeton University, Princeton, 1961.

[6] C. E. Hermance, ""A Detailed Model of the Combustion of Composite Solid Propellants"," in *2nd Solid Propulsion Conference*, Waterloo, Ontario Canada, 1967.

[7] M. W. Beckstead, R. L. Derr and C. F. Price, ""A Model of Composite Solid-Propellant Combustion Based on Multiple Flames"," *AIAA Journal*, vol. 8, no. 12, pp. 2200-2207, 1970.

[8] R. L. Glick, "Steady-State Combustion of Nonmetallized Composite Solid Propellant," MORTON THIOKOL Corporation, U-75-27, Huntsville AL, 1975.

[9] N. S. Cohen and L. D. Strand, ""An Improved Model for the Combustion of AP Composite Propellants"," *AIAA Journal*, vol. 20, no. 12, pp. 1739-1746, 1982.

[10] J. P. Renie, J. A. Condon and J. R. Osborn, "Oxidizer Size Distribution Effects on Propellant Combustion," *AIAA Journal*, vol. 17, no. 8, pp. 877-883, 1979.

[11] N. S. Cohen and J. O. Hightower, ""An Explanation for Anomalous Combustion Behavior in Composite Propellants"," in *Proceedings of the 29th JANNAF Combustion Meeting*, Huntsville, Al, 1992.

[12] R. R. Miller, K. O. Hartman and R. B. Myers, ""Prediction of Ammonium Perchlorate Particle Size Effect on Composite Propellant Burning Rate"," in *Proceedings of 26th JANNAF Solid Propulsion Meeting*, CPIA Publication. No. 196, 1970.

[13] M. K. King, ""Model for Steady State Combustion of Unimodal Composite Solid Propellants"," in *AIAA 16th Aerospace Ssciences Meeting*, Huntsville, Al, 1978.

[14] N. S. Cohen, "Review of Composite Propellant Burn Rate Modeling," *AIAA Journal*, vol. 18, no. 3, pp. 277-294, 1980.

[15] R. R. Miller, ""Effects of Particle Size on Reduced Smoke Propellant Ballistics"," in *AIAA/SAE/ASME 18th Joint Propulsion Conference*, Cleveland, Oh, 1982.

[16] N. S. Cohen and L. D. Strand, ""An Improved Model for the Combustion of AP Composite Propellants"," *AIAA Journal*, vol. 20, no. 12, pp. 1739-1747, 1982.

[17] C. A. Fraizer, "Modeling Solid Propellant Strand Burner Experiments with Catalytic Nanoparticle Additives," PhD Dissertation, Mechanical Engineering,Texas A&M University, College Station, 2011.

[18] J. A. Steinz and P. L. Stang, "The Burning Mechanism of Ammonium Perchlorate-Based Composite Solid Propellants," in *AIAA 4th Propulsion Join Specialist Conference*, Cleveland, OH, 1968.

[19] C. W. Fong and R. F. Smith, "The Relationship between Plateau Burning Behavior and Ammonium Perchlorate Particle Size in HTPB-AP Composite Propellants," in *Combustion and Flame 67:* pp. 235-247, Adelaide, South Australia, 1987.

[20] M. A. Stephens, "Tailoring the Plateau Burning Rates of Composite Propellants by the use of Nanoscale Additives," Thesis, Mechanical Engineering, Texas A&M University, College Station, 2009.

[21] T. L. Boggs, R. L. Deer and M. W. Beckstead, "Surface Structure of Ammonium Perchlorate Composite Propellants," *AIAA Journal*, vol. 8, no. 2, pp. 370-373, 1970.

[22] M. Kohga, "Burning Characteristics and Thermochemical Behavior of AP/HTPB Composite Propellant Using Coarse and Fine AP Particles," *Propellants, Explosives and Pyrotechnics*, vol. 36, no. 1, pp. pp. 57-64, 2011.

[23] M. K. King, "A Model of the Effects of Pressure and Crossflow Velocity on Composite Propellant Burning Rate," in *15th AIAA Joint Propulsion Conference, AIAA Paper No. 1979-1171*, Las Vegas, NV, July 18-20, 1979, 1979.

[24] R. L. Foster, J. A. Condon and R. R. Miller, "Low Exponent Technology," Hercules

Report, AFRRPL-TR-81-95, Hercules, Inc., Air Force Rocket Propulsion Laboratory, Edwards AFB, CA, 1982.

[25] M. Stephens, T. Sammet, R. Carro, A. LePage and E. Petersen, "Comparison of Hand and Mechanically Mixed AP/HTPB Solid Composite Propellant," in *43rd AIAA/ASME/SAE/ASEE Joint Propulsion Conference*, Cincinnati, OH, 2007.

[26] R. Carro, M. Stephens, J. Arvanetes, A. Powell and E. Petersen, "High-Pressure Testing of Composite Solid Propellant Mixtures: Burner Facility Characterization," in *41st AIAA/ASME/SAE/ASEE Joint Propulsion Conference & Exhibit*, Tuscan Arizona, 2005.

[27] R. V. Carro, "High Pressure Testing of Composite Solid Rocket Propellant Mixtures: Burner Facility Characterization," Thesis, Mechanical and Aerospace Engineering, University of Central Floridia, Orlando, FL, 2007.

[28] R. Bellec, J. Duterque and G. Lengelle, "Modeling of Aluminized Solid Propellants," ONERA, Technical Report RT 37/7128 EN, Palaiseau, France, 1996.

[29] E. Rochford, "Temperature Sensitivity Measurements of Solid Rocket Propellants," M. S. E. Thesis, The University of Alabama, Huntsville, Spring, 1999.

[30] S. Hayakawa, M. Tanaka and C. Nakao, "An Effect of Oxidizer Particle Size on Combustion Stability in Composite Propellants," in *36th AIAA Joint Propulsion Conference, AIAA Paper No. 2000-3700*, Huntsville, AL, July 16-19, 2000.

[31] R. Frederick and J. R. Osborn, "Ballistic Studies of Wide Distribution Propellants," in *36th AIAA Joint Propulsion Conference, AIAA Paper No. 2000-3318*, Huntsville,

AL, July 17-19, 2000.

[32] A. I. Atwood, K. P. Ford and C. J. Wheeler, "High-Pressure Burning rate Studies of Solid Rocket Propellants," *Progress in Propulsion Physics 4,* vol. 3, no. 13, 2013.

[33] T. L. Boggs, "Deflagration Rate, Surface Structure, and Subsurface Profile of Self-Deflagrating Single Crystals of Ammonium Perchlorate," *AIAA Journal,* vol. 8, no. 5, pp. pp. 867-973, 1970.

APPENDIX A

RAW BURNING RATE DATA COLLECTED AT TAMU

Solids Loading	AP Size	Pressure		Burning Rate	
	(μm)	(MPa)	(psia)	(mm/s)	(in/s)
0.80	20	4.2	608	13.7	0.539
0.80	20	4.5	654	15.7	0.619
0.80	20	5.8	843	17.9	0.705
0.80	20	6.8	989	16.8	0.663
0.80	20	6.8	993	17.7	0.697
0.80	20	8.3	1197	19.1	0.751
0.80	20	9.1	1315	20.7	0.816
0.80	20	10.2	1474	23.0	0.907
0.80	20	11.9	1725	27.3	1.075
0.80	20	12.5	1820	25.0	0.985
0.80	20	14.6	2111	27.7	1.091
0.80	20	14.9	2155	32.7	1.286
0.80	45	4.1	594	14.3	0.564
0.80	45	4.8	691	16.6	0.654
0.80	45	5.8	844	15.9	0.626
0.80	45	6.0	865	17.2	0.675
0.80	45	6.9	1003	17.9	0.703
0.80	45	7.9	1143	19.3	0.759
0.80	45	9.6	1390	20.3	0.801
0.80	45	11.2	1619	23.3	0.918
0.80	45	12.9	1868	24.9	0.981
0.80	45	14.6	2118	23.2	0.911
0.80	138	4.5	658	9.5	0.372
0.80	138	6.0	864	10.0	0.395
0.80	138	7.9	1148	10.5	0.414
0.80	138	9.1	1319	10.6	0.416
0.80	138	11.0	1601	11.5	0.453
0.80	138	12.8	1851	11.5	0.452
0.80	138	14.6	2121	11.4	0.450

Solids Loading	AP Size	Pressure		Burning Rate	
	(μm)	(MPa)	(psia)	(mm/s)	(in/s)
0.80	200	4.2	605	6.3	0.246
0.80	200	6.1	885	7.2	0.283
0.80	200	6.7	968	7.6	0.301
0.80	200	7.8	1132	7.9	0.313
0.80	200	7.9	1141	7.6	0.297
0.80	200	9.4	1368	8.1	0.320
0.80	200	11.2	1623	7.5	0.297
0.80	200	12.9	1875	8.2	0.323
0.80	200	14.7	2130	8.5	0.335
0.85	200	4.1	599	6.2	0.244
0.85	200	4.3	618	6.7	0.264
0.85	200	5.0	722	7.6	0.300
0.85	200	5.2	749	6.9	0.271
0.85	200	5.9	862	7.5	0.296
0.85	200	6.1	881	8.2	0.322
0.85	200	6.9	996	7.7	0.303
0.85	200	7.8	1130	7.5	0.296
0.85	200	8.0	1159	7.7	0.303
0.85	200	8.4	1219	8.1	0.318
0.85	200	9.4	1364	7.8	0.307
0.85	200	9.4	1367	8.4	0.331
0.85	200	11.6	1676	9.0	0.354
0.85	200	12.9	1865	9.9	0.388
0.85	200	14.6	2123	9.1	0.359
0.85	200	14.8	2152	9.8	0.386
0.77	200	4.0	584	5.6	0.219
0.77	200	4.9	705	6.2	0.245
0.77	200	5.8	839	6.4	0.253
0.77	200	7.4	1080	6.6	0.260
0.77	200	7.6	1106	7.2	0.285
0.77	200	9.3	1348	7.1	0.280
0.77	200	11.0	1595	7.2	0.285
0.77	200	12.8	1863	6.8	0.268
0.77	200	14.5	2105	7.0	0.275

Solids Loading	AP Size	Pressure		Burning Rate	
	(µm)	(MPa)	(psia)	(mm/s)	(in/s)
0.75	200	3.9	566	6.2	0.245
0.75	200	4.2	614	5.9	0.233
0.75	200	4.6	669	5.9	0.234
0.75	200	5.9	854	6.2	0.244
0.75	200	7.5	1086	6.8	0.267
0.75	200	9.2	1337	6.6	0.260
0.75	200	11.0	1591	6.7	0.263
0.75	200	12.5	1819	6.7	0.262
0.70	200	4.5	651	4.5	0.178
0.70	200	5.2	747	4.8	0.189
0.70	200	6.1	891	5.2	0.204
0.70	200	8.1	1179	5.7	0.225
0.70	200	9.9	1443	5.9	0.234
0.70	200	11.7	1691	5.7	0.225
0.70	200	13.2	1909	5.3	0.211
0.70	200	15.2	2204	5.5	0.218
0.80	75	4.5	647	10.2	0.402
0.80	75	5.6	815	12.0	0.472
0.80	75	8.4	1215	14.9	0.587
0.80	75	9.9	1441	15.0	0.592
0.80	75	11.7	1703	15.8	0.621
0.80	75	13.5	1953	18.7	0.738

APPENDIX B

APPROXIMATE RAW BURNING RATE DATA COLLECTED FROM KOHGA [22]

Solids Loading	AP Size	Pressure		Burning Rate	
	(μm)	(MPa)	(psia)	(mm/s)	(in/s)
0.55	110	1.5	218	0.36	0.014
0.55	110	2	290	0.43	0.017
0.56	110	1	145	0.34	0.013
0.56	110	1.5	218	0.44	0.017
0.56	110	2	290	0.52	0.020
0.60	110	1	145	0.52	0.020
0.60	110	1.5	218	0.68	0.027
0.60	110	2	290	0.83	0.033
0.60	110	2.5	363	0.90	0.035
0.60	110	3	435	0.92	0.036
0.62	110	1	145	0.86	0.034
0.62	110	1.5	218	1.10	0.043
0.62	110	2	290	1.32	0.052
0.62	110	3	435	1.61	0.063
0.62	110	4	580	1.82	0.072
0.63	110	1	145	0.94	0.037
0.63	110	1.5	218	1.18	0.046
0.63	110	2	290	1.43	0.056
0.63	110	3	435	1.77	0.070
0.63	110	4	580	2.04	0.080
0.63	110	5	725	2.23	0.088
0.63	110	6	870	2.34	0.092
0.63	110	7	1015	2.34	0.092
0.64	110	0.5	73	0.72	0.028
0.64	110	1	145	1.02	0.040
0.64	110	2	290	1.53	0.060
0.64	110	3	435	1.91	0.075
0.64	110	5	725	2.36	0.093
0.64	110	7	1015	2.53	0.100

Solids Loading	AP Size	Pressure		Burning Rate	
	(μm)	(MPa)	(psia)	(mm/s)	(in/s)
0.70	110	0.5	73	1.29	0.051
0.70	110	1	145	1.69	0.067
0.70	110	2	290	2.30	0.091
0.70	110	3	435	2.56	0.101
0.70	110	5	725	3.08	0.121
0.70	110	7	1015	3.48	0.137
0.75	110	0.5	73	2.04	0.080
0.75	110	1	145	2.53	0.100
0.75	110	2	290	3.15	0.124
0.75	110	3	435	3.77	0.148
0.75	110	5	725	4.43	0.174
0.75	110	7	1015	4.97	0.196
0.80	110	0.5	73	2.62	0.103
0.80	110	1	145	3.45	0.136
0.80	110	2	290	4.40	0.173
0.80	110	3	435	5.09	0.200
0.80	110	5	725	6.08	0.239
0.80	110	7	1015	7.04	0.277
0.63	4	2	290	1.70	0.067
0.63	4	2.5	363	1.91	0.075
0.63	4	3	435	2.02	0.080
0.64	4	1.5	218	1.70	0.067
0.64	4	2	290	2.11	0.083
0.64	4	3	435	2.40	0.094
0.64	4	4	580	2.69	0.106
0.66	4	1	145	1.78	0.070
0.66	4	1.5	218	2.32	0.091
0.66	4	2	290	2.74	0.108
0.66	4	3	435	3.19	0.126
0.66	4	5	725	3.89	0.153
0.68	4	1	145	2.32	0.091
0.68	4	1.5	218	2.81	0.111
0.68	4	2	290	3.15	0.124
0.68	4	3	435	3.76	0.148
0.68	4	5	725	4.66	0.183
0.68	4	6	870	4.85	0.191

Solids Loading	AP Size	Pressure		Burning Rate	
	(μm)	(MPa)	(psia)	(mm/s)	(in/s)
0.69	4	0.5	73	1.93	0.076
0.69	4	1	145	2.52	0.099
0.69	4	2	290	3.36	0.132
0.69	4	3	435	3.99	0.157
0.69	4	5	725	4.85	0.191
0.69	4	7	1015	5.31	0.209
0.70	4	0.5	73	2.06	0.081
0.70	4	1	145	2.69	0.106
0.70	4	2	290	3.50	0.138
0.70	4	3	435	4.22	0.166
0.70	4	5	725	5.14	0.202
0.70	4	7	1015	5.90	0.232
0.75	4	0.5	73	3.17	0.125
0.75	4	1	145	4.29	0.169
0.75	4	2	290	5.90	0.232
0.75	4	3	435	6.46	0.254
0.75	4	5	725	8.05	0.317
0.75	4	7	1015	9.40	0.370
0.80	4	0.5	73	6.67	0.263
0.80	4	1	145	9.40	0.370
0.80	4	2	290	13.47	0.530
0.80	4	3	435	15.86	0.624
0.80	4	5	725	20.27	0.798
0.80	4	7	1015	23.86	0.939

APPENDIX C

APPROXIMATE RAW BURNING RATE DATA COLLECTED FROM KING [23]

Solids Loading	AP Size	Pressure		Burning Rate	
	(μm)	(MPa)	(psia)	(mm/s)	(in/s)
0.73	200	1.0	147	2.02	0.079
0.73	200	3.0	441	2.94	0.116
0.73	200	4.1	588	4.38	0.173
0.73	200	6.1	882	5.38	0.212
0.73	200	10.1	1470	6.99	0.275
0.73	200	15.2	2204	8.80	0.346
0.73	20	1.0	147	3.02	0.119
0.73	20	3.0	441	4.53	0.178
0.73	20	4.1	588	6.34	0.249
0.73	20	6.1	882	7.83	0.308
0.73	20	10.1	1470	11.66	0.459
0.73	20	15.2	2204	14.40	0.567
0.73	5	1.0	147	3.02	0.119
0.73	5	3.0	441	5.33	0.210
0.73	5	4.1	588	10.24	0.403
0.73	5	6.1	882	14.07	0.554
0.73	5	10.1	1470	18.39	0.724
0.73	5	15.2	2204	22.29	0.878
0.77	20	0.7	100	3.56	0.140
0.77	20	1.4	202	6.19	0.244
0.77	20	2.1	304	7.70	0.303
0.77	20	3.4	499	8.93	0.352
0.77	20	5.1	746	10.90	0.429
0.77	20	7.0	1008	12.81	0.504
0.77	20	8.5	1233	14.24	0.561
0.77	20	10.5	1527	15.53	0.612
0.77	20	13.9	2014	18.15	0.714

APPENDIX D

APPROXIMATE RAW BURNING RATE DATA COLLECTED FROM FOSTER [24]

Solids Loading	AP Size	Pressure		Burning Rate	
	(μm)	(MPa)	(psia)	(mm/s)	(in/s)
0.75	12	0.7	100	2.78	0.110
0.75	12	2.1	300	6.06	0.238
0.75	12	3.4	500	7.80	0.307
0.75	12	6.9	1000	11.10	0.437
0.75	12	13.8	2000	19.69	0.775
0.75	12	20.7	3000	27.64	1.088
0.775	12	0.7	100	3.35	0.132
0.775	12	2.1	300	8.69	0.342
0.775	12	3.4	500	11.98	0.472
0.775	12	6.9	1000	16.43	0.647
0.775	12	6.9	1000	15.74	0.620
0.775	12	13.8	2000	24.25	0.955
0.775	12	20.7	3000	35.10	1.382
0.80	12	0.7	100	4.38	0.173
0.80	12	2.1	300	12.25	0.482
0.80	12	3.4	500	16.58	0.653
0.80	12	6.9	1000	23.02	0.906
0.80	12	13.8	2000	31.95	1.258
0.80	12	20.7	3000	42.70	1.681

APPENDIX E

APPROXIMATE RAW BURNING RATE DATA COLLECTED FROM BELLEC [28]

Solids Loading	AP	Pressure		Burning Rate		Pressure		Burning Rate	
	(um)	(MPa)	(psia)	(mm/s)	(in/s)	(MPa)	(psia)	(mm/s)	(in/s)
80.0%	5	0.9	129	6.5	0.255	9.6	1400	51.6	2.031
		1.2	173	7.8	0.308	11.8	1710	56.0	2.206
		1.6	230	11.2	0.439	14.5	2110	59.5	2.342
		2.1	304	14.9	0.585	14.6	2122	62.9	2.478
		2.5	360	20.5	0.806	17.2	2493	64.3	2.531
		2.9	422	22.2	0.876	17.2	2500	67.3	2.649
		3.1	447	21.7	0.854	19.0	2763	67.7	2.666
		3.4	493	26.3	1.034	19.4	2815	70.7	2.783
		3.6	522	25.3	0.997	21.2	3075	75.4	2.968
		4.1	588	27.1	1.069	21.4	3098	67.3	2.648
		4.8	693	34.8	1.371	22.3	3229	71.3	2.809
		4.8	701	30.3	1.193	24.2	3515	86.6	3.411
		5.8	846	39.5	1.557	24.7	3578	73.3	2.884
		5.9	861	37.5	1.475	24.7	3587	69.1	2.719
		6.8	987	42.4	1.669	33.5	4864	88.5	3.483
		6.9	998	40.5	1.596	33.8	4904	94.0	3.699
		7.3	1055	45.0	1.772	48.3	7001	108.1	4.256
		7.6	1108	45.4	1.789	66.3	9616	164.2	6.463
		8.0	1158	48.3	1.900	69.4	10071	152.5	6.003
		8.7	1265	54.3	2.137	94.5	13706	178.3	7.018
		8.8	1275	47.3	1.862	95.0	13783	188.8	7.435

Solids Loading	AP	Pressure		Burning Rate		Pressure		Burning Rate	
	(um)	(MPa)	(psia)	(mm/s)	(in/s)	(MPa)	(psia)	(mm/s)	(in/s)
80%	90	0.6	80	3.00	0.118	7.5	1086	9.35	0.368
		1.0	145	3.65	0.144	8.1	1169	10.12	0.398
		1.3	187	4.10	0.161	9.1	1322	10.67	0.420
		1.4	199	4.71	0.185	9.9	1441	10.99	0.433
		1.6	228	4.80	0.189	10.2	1478	10.46	0.412
		1.8	259	4.89	0.192	11.9	1732	11.25	0.443
		2.0	289	5.16	0.203	14.2	2055	12.23	0.481
		2.1	303	4.96	0.195	14.8	2145	13.77	0.542
		2.1	304	5.74	0.226	15.9	2301	12.66	0.498
		2.1	310	5.37	0.211	16.2	2349	13.96	0.550
		3.0	437	6.38	0.251	18.0	2616	14.28	0.562
		3.1	452	6.91	0.272	19.8	2877	16.00	0.630
		3.1	454	5.93	0.233	19.9	2884	14.96	0.589
		4.0	576	6.72	0.265	21.9	3176	17.17	0.676
		4.1	590	7.29	0.287	24.8	3599	16.69	0.657
		4.2	603	7.66	0.302	25.0	3626	20.44	0.805
		4.5	658	7.69	0.303	28.9	4185	19.06	0.750
		4.7	676	8.33	0.328	29.9	4335	22.23	0.875
		4.9	712	8.01	0.315	34.6	5012	22.20	0.874
		5.0	719	7.59	0.299	34.6	5022	26.00	1.024
		5.2	753	8.77	0.345	39.6	5738	26.63	1.048
		5.2	756	8.10	0.319	39.8	5766	23.32	0.918
		5.4	781	7.71	0.304	44.8	6498	30.00	1.181
		5.6	807	8.45	0.333	45.0	6527	24.47	0.963
		5.7	820	8.90	0.350	49.5	7177	27.41	1.079
		5.9	861	7.96	0.313	49.8	7218	29.43	1.159
		6.0	868	8.68	0.342	50.0	7250	32.68	1.287
		6.3	919	8.49	0.334	54.9	7963	37.46	1.475
		6.4	931	8.19	0.322	59.7	8661	39.95	1.573
		6.5	948	9.14	0.360	70.2	10186	50.70	1.996
		7.0	1016	8.64	0.340	80.4	11660	60.34	2.376
		7.0	1019	9.51	0.375	90.3	13097	66.53	2.619
						98.5	14288	74.55	2.935

APPENDIX F

APPROXIMATE RAW BURNING RATE DATA COLLECTED FROM ROCKFORD [28]

AP	Pressure		Burning Rate		Pressure		Burning Rate	
(um)	(MPa)	(psia)	(mm/s)	(in/s)	(MPa)	(psia)	(mm/s)	(in/s)
17	0.6	88	4.2	0.166	5.1	740	7.9	0.312
	0.9	133	4.6	0.181	5.4	779	8.2	0.322
	1.1	162	4.5	0.178	5.7	820	8.5	0.334
	1.3	184	5.0	0.196	5.9	861	8.8	0.346
	1.5	211	5.3	0.211	6.2	905	9.1	0.359
	1.6	239	5.6	0.221	6.6	952	9.4	0.369
	1.9	269	5.9	0.231	6.9	1000	9.7	0.383
	2.1	301	6.1	0.239	7.3	1052	10.1	0.399
	2.3	336	6.3	0.247	7.6	1108	10.5	0.414
	2.6	371	6.4	0.252	8.0	1167	10.9	0.429
	2.8	408	6.6	0.259	8.4	1225	11.2	0.443
	3.1	445	6.7	0.263	8.9	1288	11.7	0.462
	3.3	480	6.5	0.258	9.3	1348	12.3	0.482
	3.5	515	6.6	0.261	9.8	1417	12.8	0.503
	3.8	546	6.8	0.266	10.2	1486	13.1	0.516
	4.0	573	6.9	0.272	10.9	1577	13.5	0.530
	4.2	603	7.0	0.275	11.7	1692	14.0	0.553
	4.4	635	7.2	0.284	12.8	1860	15.1	0.593
	4.6	669	7.5	0.295	14.5	2103	16.2	0.638
	4.8	702	7.7	0.302	16.3	2359	17.3	0.682

AP	Pressure		Burning Rate	
(um)	(MPa)	(psia)	(mm/s)	(in/s)
90	1.1	158	1.9	0.075
	1.3	183	2.2	0.085
	1.5	216	2.5	0.097
	1.7	248	3.0	0.118
	1.9	278	3.1	0.122
	2.1	308	3.2	0.125
	2.4	343	3.3	0.129
	2.6	380	3.4	0.135
	2.9	420	3.7	0.144
	3.2	463	3.9	0.152
	3.5	507	4.2	0.164
	3.8	554	4.4	0.175
	4.2	604	4.5	0.176
	4.5	653	4.5	0.176
	4.9	708	4.6	0.180
	5.3	763	4.8	0.190
	5.6	810	4.9	0.193
	5.9	854	5.0	0.198
	6.2	894	5.1	0.202
	6.5	937	5.1	0.202
	6.8	983	5.0	0.198
	7.1	1028	5.0	0.198
	7.4	1074	5.3	0.207
	7.7	1121	5.4	0.212

APPENDIX G

APPROXIMATE RAW BURNING RATE DATA COLLECTED FROM HAYAWAKA [30]

Solids Loading	AP	Pressure		Burning Rate	
	(um)	(MPa)	(psia)	(mm/s)	(in/s)
73.0%	50	0.7	104	2.05	0.081
		0.9	127	2.21	0.087
		1.4	203	2.52	0.099
		1.6	232	2.58	0.102
		1.7	252	2.61	0.103
		2.0	292	2.86	0.113
		2.5	363	2.80	0.110
		3.2	460	3.35	0.132
		3.4	497	3.44	0.135
		4.2	603	4.03	0.159
		4.5	654	4.17	0.164
		5.3	769	4.80	0.189
		6.2	900	5.46	0.215
		6.7	972	5.72	0.225
		8.2	1185	6.67	0.263
		9.6	1395	7.49	0.295
73.0%	15	0.6	82	1.89	0.074
		0.8	115	2.32	0.091
		1.2	170	2.65	0.104
		1.6	237	3.03	0.119
		2.1	299	3.56	0.140
		2.7	393	3.59	0.141
		2.7	398	3.66	0.144
		8.5	1234	7.32	0.288
		8.8	1284	7.77	0.306
		9.6	1398	8.82	0.347
		9.8	1426	9.12	0.359

Solids Loading	AP	Pressure		Burning Rate	
	(um)	(MPa)	(psia)	(mm/s)	(in/s)
75	15	0.5	75	1.56	0.062
		0.6	91	2.00	0.079
		0.6	93	2.13	0.084
		0.7	100	2.06	0.081
		0.7	107	2.16	0.085
		1.1	153	2.89	0.114
		1.1	164	3.17	0.125
		1.5	220	3.32	0.131
		1.9	275	3.53	0.139
		2.2	313	3.58	0.141
		2.2	325	3.74	0.147
		2.5	369	3.81	0.150
		2.9	425	4.13	0.162
		3.0	438	4.11	0.162
		10.0	1446	7.60	0.299
		10.0	1452	8.51	0.335
78	15	0.7	103	2.90	0.114
		1.1	159	4.03	0.159
		1.5	213	4.37	0.172
		2.1	305	5.09	0.200
		3.1	446	5.76	0.227
		3.3	480	5.83	0.229
		3.6	515	5.97	0.235
		3.7	530	5.80	0.228
		6.1	882	8.00	0.315
		7.2	1045	11.88	0.468
		8.2	1184	12.64	0.497
		10.0	1444	14.44	0.568

Solids Loading	AP	Pressure		Burning Rate	
	(um)	(MPa)	(psia)	(mm/s)	(in/s)
80	15	1.0	147	4.68	0.184
		1.3	188	5.31	0.209
		1.8	255	5.95	0.234
		2.3	336	6.88	0.271
		2.4	342	7.04	0.277
		2.9	425	7.86	0.309
		3.1	454	8.11	0.319
		3.9	571	8.59	0.338
		4.3	630	9.24	0.364
		5.3	773	10.84	0.427
		6.2	905	11.83	0.466
		7.2	1044	13.35	0.525
		9.1	1314	15.88	0.625
		10.3	1494	17.45	0.687

APPENDIX H

APPROXIMATE RAW BURNING RATE DATA COLLECTED FROM FREDERICK [31]

AP: 16 µm				
Solids Loading	Pressure		Burning Rate	
	(MPa)	(psia)	(mm/s)	(in/s)
66.7%	1.7	250	1.98	0.078
75%	1.7	250	3.86	0.152
	3.4	500	4.80	0.189
	6.9	1000	6.22	0.245
	13.8	2000	9.25	0.364
80%	1.7	250	4.72	0.186
	3.4	500	6.30	0.248
	6.9	1000	9.22	0.363
	13.8	2000	13.59	0.535